Mon. Not. R. Astron. Soc. **367,** 349–365 (2006) doi:10.1111/j.1365-2966.2006.09967.x

Probing the evolution of the near-infrared luminosity function of galaxies to $z \simeq 3$ in the *Hubble Deep Field*-South

P. Saracco,[1⋆] A. Fiano,[1,2] G. Chincarini,[1,2] E. Vanzella,[3] M. Longhetti,[1] S. Cristiani,[4] A. Fontana,[5] E. Giallongo[5] and M. Nonino[4]

[1]*INAF – Osservatorio Astronomico di Brera, Via Brera 28, 20121 Milano, Italy*
[2]*Università degli Studi di Milano–Bicocca, P.za dell'Ateneo Nuovo 1, 20126 Milano, Italy*
[3]*European Southern Observatory, Karl-Schwarzschild-Strasse, 2, D-85748 Garching bei Munchen, Germany*
[4]*INAF – Osservatorio Astronomico di Trieste, Via Tiepolo 11, 34131 Trieste, Italy*
[5]*INAF – Osservatorio Astronomico di Roma, Via di Frascati 33, 00040 Monte Porzio Catone, Italy*

Accepted 2005 December 2. Received 2005 November 28; in original form 2005 October 10

ABSTRACT

We present the rest-frame J_s- and K_s-band luminosity function (LF) of a sample of about 300 galaxies selected in the *Hubble Deep Field*-South (HDF-S) at $K_s \leqslant 23$ (Vega). We use calibrated photometric redshift together with spectroscopic redshift for 25 per cent of the sample. The accuracy reached in the photometric redshift estimate is 0.06 (rms) and the fraction of outliers is 1 per cent. We find that the rest-frame J_s-band luminosities obtained by extrapolating the observed J_s-band photometry are consistent with those obtained by extrapolating the photometry in the redder H and K_s bands closer to the rest-frame J_s, at least up to $z \sim 2$. Moreover, we find no significant differences among the luminosities obtained with different spectral libraries. Thus, our LF estimate is not dependent either on the extrapolation made on the best-fitting template or on the library of models used to fit the photometry. The selected sample has allowed us to probe the evolution of the LF in the three redshift bins [0; 0.8), [0.8; 1.9) and [1.9; 4) centred at the median redshift $z_m \simeq [0.6, 1.2, 3]$ and to probe the LF at $z_m \simeq 0.6$ down to the unprecedented faint luminosities $M_{J_s} \simeq -13$ and $M_{K_s} \simeq -14$. We find hints of a rise of the faint-end ($M_{J_s} > -17$ and $M_{K_s} > -18$) near-infrared (near-IR) LF at $z_m \sim 0.6$: a rise that cannot be probed at higher redshift with our sample. The values of α we estimate are consistent with the local value and do not show any trend with redshift. We do not see evidence of evolution from $z = 0$ to $z_m \sim 0.6$ suggesting that the population of local bright galaxies was already formed at $z < 0.8$. In contrast, we clearly detect an evolution of the LF to $z_m \sim 1.2$ characterized by a brightening of M^* and by a decline of ϕ^*. To $z_m \sim 1.2$, M^* brightens by about 0.4–0.6 mag and ϕ^* decreases by a factor 2–3. This trend persists, even if at a lesser extent, down to $z_m \sim 3$ in both the J_s- and K_s-band LF. The decline of the number density of bright galaxies seen at $z > 0.8$ suggests that a significant fraction of them increase their stellar mass at $1 < z < 2$–3 and that they underwent a strong evolution in this redshift range. On the other hand, this implies also that a significant fraction of local bright/massive galaxies were already in place at $z > 3$. Thus, our results suggest that the assembly of massive galaxies is spread over a large redshift range and that the increase of their stellar mass has been very efficient also at very high redshift at least for a fraction of them.

Key words: galaxies: evolution – galaxies: formation – galaxies: luminosity function, mass function.

1 INTRODUCTION

The luminosity function (LF) of galaxies is a fundamental statistical tool to study the populations of galaxies. Its dependence on morphological type, wavelength and look-back time provides

⋆E-mail: saracco@brera.mi.astro.it

constraints on the evolution of the properties of the whole population of galaxies, of the populations of various morphological types and on their contribution to the luminosity density at different wavelengths. The parameters derived by the best-fitting of the LF, the characteristic luminosity M^*, the slope α and the normalization ϕ^* provide strong constraints to the models of galaxy formation.

The recent estimates of the LF based on local wide surveys in the optical, such as the Two-Degree Field (2dF; Folkes et al. 1999; Madgwick et al. 2002; Norberg et al. 2002) and the Sloan Digital Sky Survey (SDSS; Blanton et al. 2003), and in the near-infrared (near-IR), such as the Two-Micron All Sky Survey (2MASS; Kochanek et al. 2001), have provided a comprehensive view of the local LF for different morphological types and wavelengths. It is now well established that the LF depends on morphological type, that the faint end is increasingly dominated by galaxies with late-type morphology and spectra and that their number density increases towards lower luminosities. In contrast, the bright end is dominated by early-type galaxies whose fraction increases with luminosities (e.g. Marzke et al. 1994, 1998; Folkes et al. 1999; Kochanek et al. 2001; Bell et al. 2003).

The studies of the LF based on optically selected redshift surveys at $z < 1$ have provided the first evidence of a differential evolution of galaxies. Lilly et al. (1995a), using the Canada–France Redshift Survey (CFRS; Lilly et al. 1995b), show that the rest-frame *B*-band LF of the blue population of galaxies brightens by about 1 mag to $z \sim 1$ contrary to the red population, which shows a little evolution over the redshift range probed. They used the observed *I*-band photometry to derive the rest-frame *B*-band luminosities. Subsequent studies confirmed the different behaviours followed by the LF of the different populations of galaxies at various redshifts (e.g. Lin et al. 1997; Liu et al. 1998) and the differential evolution they underwent (e.g. Wolf et al. 2003; Bell et al. 2004). At higher redshift ($z > 1$), the studies of the LF in the optical rest frame confirm the presence of the bimodality and provide evidence of luminosity and of density evolution down to $z \sim 2$–3 (e.g. Poli et al. 2003; Gabasch et al. 2004; Giallongo et al. 2005).

Contrary to the light at UV and optical wavelengths, the near-IR light is less affected by dust extinction and ongoing star formation (e.g. Rix & Riecke 1993; Kauffmann & Charlot 1998). Moreover, because the near-IR light of a galaxy is dominated by the evolved population of stars, the near-IR light is weakly dependent on galaxy type and is more related to the stellar mass of the galaxy. Therefore, the evolution of the LF of galaxies in the near-IR rest frame can provide important clues on the history of the stellar mass assembly in the Universe rather than on the evolution of the star formation.

The studies of the *K*-band LF conducted so far have shown no or little evolution of the population of galaxies at $z < 0.4$–0.5 (e.g. Glazebrook et al. 1995; Feulner et al. 2003; Pozzetti et al. 2003) with respect to the local population (Glazebrook et al. 1995; Gardner et al. 1997; Cole et al. 2001; Kochanek et al. 2001). In contrast, evidence of evolution emerges at $z > 0.5$, even if some discrepancies are present among the results obtained by the various authors (see e.g. Cowie et al. 1996; Drory et al. 2003; Pozzetti et al. 2003; Caputi et al. 2004, 2005a; Dahlen et al. 2005). One of the possible reasons for these discrepancies is related to the rest-frame *K*-band luminosities, usually extrapolated from the observed *K*-band photometry making use of the best-fitting template which should reproduce the unknown spectral energy distribution (SED) of the galaxy. To minimize the uncertainties, photometry at wavelengths longwards the rest-frame *K* band would be required. Given the obvious difficulties in getting deep mid-IR observations, some authors have used the observed *K*-band magnitudes to construct the rest-frame *J*-band LF (e.g. Bolzonella, Pellò & Maccagni 2002; Pozzetti et al. 2003; Dahlen et al. 2005) and to constrain the evolution of the LF in the near-IR. Another reason could be that deep *K*-band observations allowing a good sampling of the LF at magnitudes fainter than M^* over a wide redshift range are not so common. Consequently, the LF faintwards of the knee is progressively less constrained with increasing redshift affecting the LF estimate.

In this work, we aim at measuring the rest-frame J_s- and K_s-band LF of galaxies and its evolution to $z \simeq 3$ through a sample of about 300 galaxies selected at $K_s \leqslant 23$ on the *Hubble Deep Field*-South (HDF-S). The extremely deep near-IR observations collected on this field coupled with the optical *Hubble Space Telescope* (*HST*) data have allowed us to probe the LF over a wide redshift range and to sample the faint end of the LF down to unprecedented faint luminosities. We use photometric redshift spectroscopically calibrated with a sample of more than 230 spectroscopic redshifts, ∼80 of which are in the HDF-S. We pay particular attention to the calculation of the rest-frame near-IR luminosities by comparing different methods and libraries of models. In Section 2, we describe the photometric catalogue and the criteria adopted to construct the final sample of galaxies used to derive the LF. In Section 3, we describe the procedure used to obtain calibrated photometric redshifts and we present the redshift and colour distribution of galaxies. In Section 4, we discuss the derivation of the rest-frame J_s- and K_s-band absolute magnitudes and assess the influence of the different estimates on the LF. The resulting LF at various redshifts is derived in Section 5. In Section 6, our LFs are compared with the local estimates and with those previously obtained by other authors at comparable redshifts to depict the evolution of the LF of galaxies up to $z \sim 3$. In Section 7, we summarize and discuss the results.

Throughout this paper, magnitudes are in the Vega system unless explicitly stated otherwise. We adopt an $\Omega_m = 0.3$, $\Omega_\Lambda = 0.7$ cosmology with $H_0 = 70$ km s^{-1} Mpc^{-1}.

2 PHOTOMETRIC CATALOGUE AND SAMPLE SELECTION

The K_s-band selected catalogue we use has been obtained by combining version 2 of the *HST* images in the U_{300}, B_{450}, V_{606} and I_{814} bands (Casertano et al. 2000) with the deep (∼30 h per filter) VLT-ISAAC (Very Large Telescope Infrared Spectrometer and Array Camera) observations centred on the HDF-S carried out in the framework of the FIRES (Faint Infrared Extragalactic Survey) project (Franx et al. 2000; Labbè et al. 2003a) in the J_s, H and K_s bands. The formal limiting magnitudes (3σ within 0.2 arcsec^2) reached are 26.7, 29.1 29.5, 28.6, 26.2, 24.5 and 24.4 in the U_{300}, B_{450}, V_{606}, I_{814}, J_s, H and K_s bands, respectively. The detection has been performed using SExtractor (Bertin & Arnouts 1996) on the K_s-band image. The K_s-band magnitude is the MAG_BEST measured by SExtractor, while the colours have been measured within the K_s-band detection isophote by using SExtractor in double image mode. The near-IR data reduction, the detection and the magnitude estimate are described in detail in Saracco et al. (2001, 2004). To construct our catalogue, we considered the area of the HDF-S fully covered by all the images in the various bands resulting in an area of ∼5.5 arcmin^2. On this area, we detected 610 sources at $K_s < 26$. In Fig. 1, the observed number counts are shown.

From this K_s-band selected catalogue, we extracted a complete sample of galaxies to derive the LF. On the basis of the simulations described in Saracco et al. (2001), we estimated that our catalogue is 100 per cent complete at $K_s \simeq 23.2$. This is consistent with the

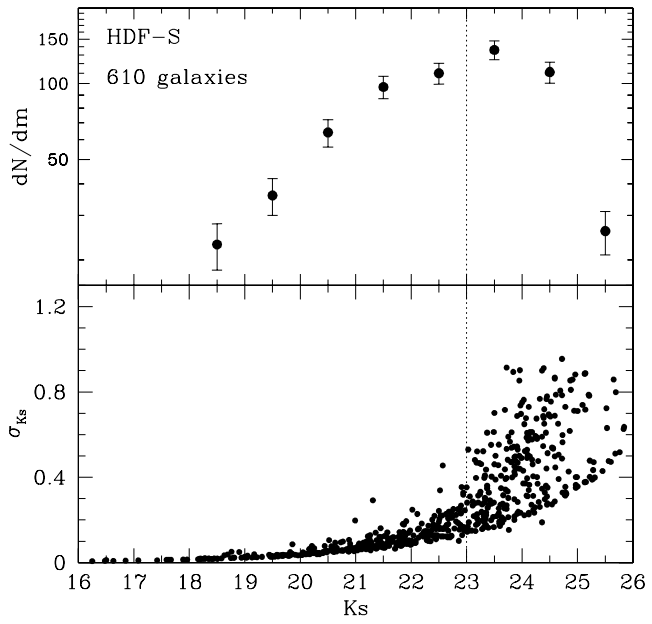

Figure 1. Upper panel: K_s-band number counts as resulting from the whole sample of 610 galaxies detected in the HDF-S. The counts increase till $K_s \simeq 24$ and drop at fainter magnitudes in agreement with the 100 per cent completeness estimated at $K_s \simeq 23.2$. Lower panel: photometric errors as a function of K_s-band magnitude for the whole sample of galaxies in the HDF-S. At $K_s \simeq 23$, the photometric error is still lower than 0.2 mag for most of the galaxies, while it is much larger at fainter magnitudes. The dotted line marks the limiting magnitude of the K23 selected sample.

number counts shown in Fig. 1 which raise till $K_s \simeq 24$. Down to $K_s \simeq 23$, the near-IR photometric errors are lower than 0.2 mag, while they rapidly increase at fainter magnitudes, as shown in the lower panel of Fig. 1, making very uncertain the photometric redshift estimate. Thus, according to these considerations, we constructed the sample by selecting all the sources (332) brighter than $K_s = 23$ (K23 sample hereafter). We then identified and removed the stars

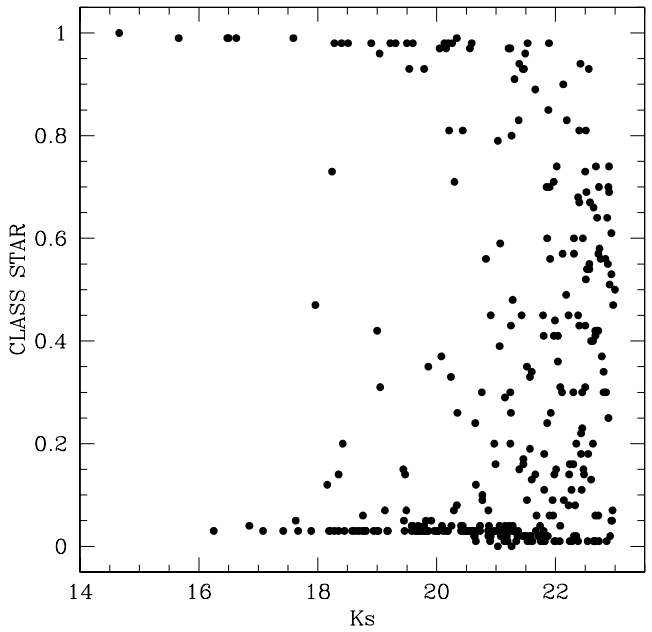

Figure 2. SExtractor stellar index (CLASS_STAR) as a function of K_s magnitude for the 332 sources brighter than $K_s = 23$.

from the K23 sample relying both on the SExtractor star/galaxy classifier and on the colours of the sources. In Fig. 2, the stellar index (CLASS_STAR) computed by SExtractor for the 332 sources of the K23 sample is shown as a function of the K_s-band apparent magnitude. For magnitudes brighter than $K_s \simeq 21$, point like sources (CLASS_STAR $\simeq 1$) and extended sources (CLASS_STAR $\simeq 0$) are well segregated, while they tend to mix at fainter magnitudes. We defined stellar candidates as those sources with magnitudes $K_s < 21$ having a CLASS_STAR >0.95 both in the K_s- and I_{814}-band images. We obtained a sample of 23 stellar candidates. Among them, seven bright ($K_s < 18.5$) sources display spikes in the *HST* Wide Field Planetary Camera (WFPC) images, implying that they are most likely stars. For the remaining 16 candidates, we verified that their optical and near-IR colours were compatible with those of stars. In Fig. 3, the colours $J_s - K_s$ and $V_{606} - I_{814}$ of the K23 sample are plotted as a function of the K_s magnitude and of the $J_s - K_s$ colour, respectively. The 16 star candidates and the seven bright stars are marked by filled points and starred symbols, respectively. As can be seen, all but two of the candidates occupy the stellar locus at $J - K < 0.9$ and are well segregated both in the colour–magnitude and colour–colour plane. In contrast, the two candidates lying far from the stellar locus of Fig. 3 display colours not compatible with those of stars. In particular, while their $J - K$ colour ($J - K > 1.3$) could be consistent with the near-IR colour of an M6–M8 spectral type, the other optical colours differ even more than 2 mag from those characterizing these stars. Thus, these two sources are most probably misclassified compact galaxies. This has made us classify 21 stars out of the 23 candidates originally selected on the basis of the SExtractor stellar index at $K_s < 21$.

At magnitudes fainter than $K_s = 21$, other sources (18) lie in the locus occupied by stars defined by a colour $J - K < 0.9$. By a visual inspection of the 18 sources on the *HST* images, we clearly identified the extended profile for seven of them. In contrast, the remaining 11 sources have an FWHM and a surface brightness profile consistent with a point-like source. We probed the stellar nature of these 11 star candidates by comparing their observed SED defined by broad-band photometry with a set of spectral templates of stellar atmospheres from the Kurucz atlas (Kurucz 1993). The observed SEDs of all the 11 star candidates are very well fitted by those of M and K stars. All but one are not targets of spectroscopic observations, as we verified through the European Southern Observatory (ESO) archive data available. The spectrum available for the remaining one J32m58.07s-32′58.9″ confirms its stellar nature as an M star. In the left panel of Fig. 4, we show the reduced χ^2 of the best-fitting template to the SED of the 18 sources with $J - K < 0.9$ obtained with the stellar atmosphere templates of Kurucz ($\tilde{\chi}^2_{\rm star}$) and with the stellar population templates of BC03 ($\tilde{\chi}^2_{\rm gal}$). It is interesting to note the effectiveness of this method in identifying stars and galaxies among faint K-selected objects. In the right panel of Fig. 4, we show, as an example, the SEDs of five out of the 11 stars together with the relevant best-fitting Kurucz templates. Therefore, we classified stars also these 11 sources and we removed a total of 32 stars from the K23 sample, which results in 300 galaxies.

3 PHOTOMETRIC REDSHIFTS

3.1 Templates selection

Photometric redshifts have been derived by comparing the observed flux densities to a set of synthetic templates based on the latest version of the Bruzual & Charlot (2003; BC03 hereafter) models. The χ^2 minimization procedure of Hyperz (Bolzonella, Miralles

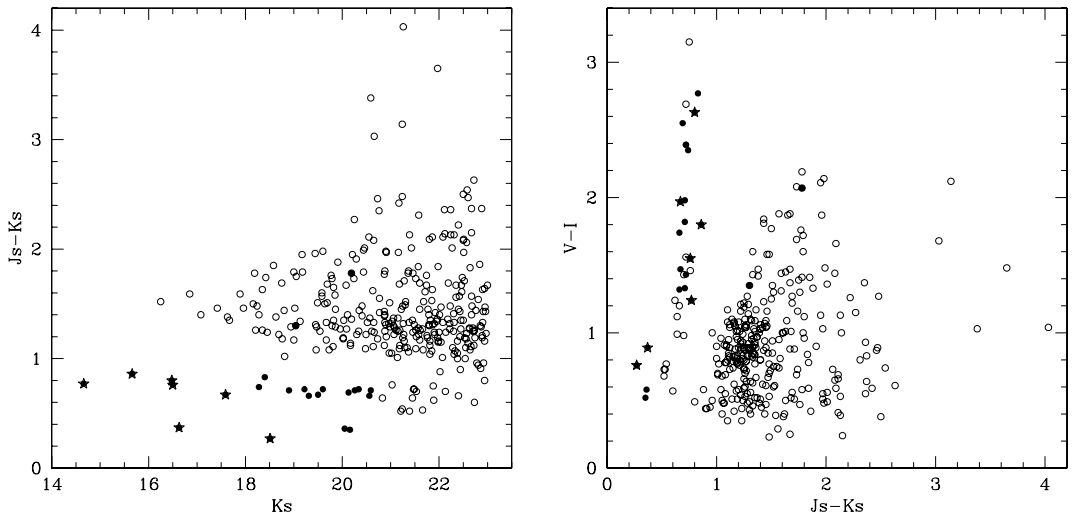

Figure 3. Colours $J_s - K_s$ (left) and $V_{606} - I_{814}$ (right) of the 332 $K_s \leqslant 23$ as a function of the K_s magnitude and $J_s - K_s$ colour, respectively. The 25 star candidates are marked as filled symbols. Among them, we marked with starred symbols those sources clearly identified as stars because they show spikes in the HDF-WFPC images.

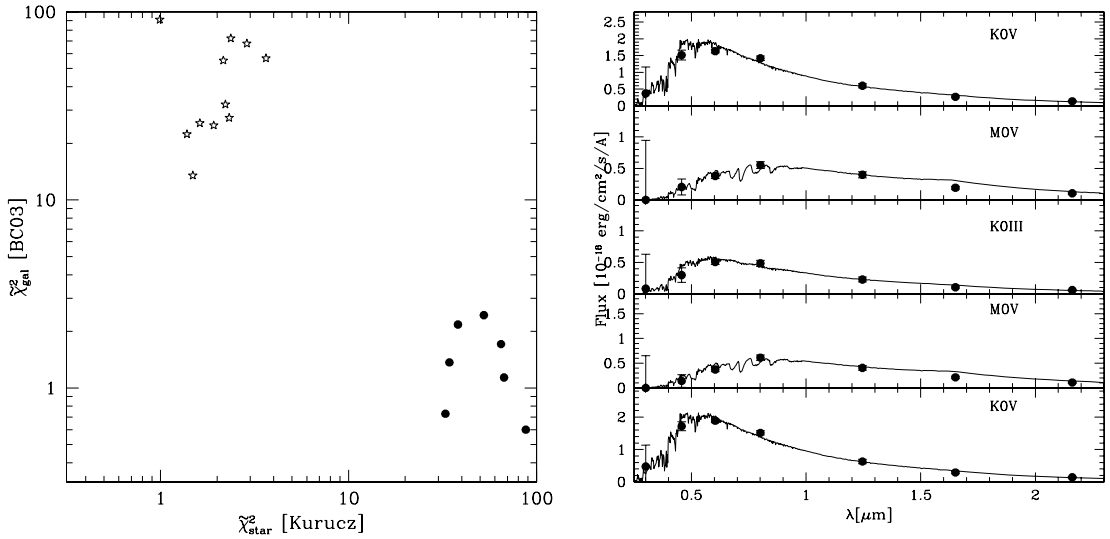

Figure 4. Left: reduced χ^2 obtained by fitting the SED of the 18 sources with $K > 21$ and $J - K < 0.9$ with the Kurucz templates ($\tilde{\chi}^2_{\rm star}$) and with stellar population templates ($\tilde{\chi}^2_{\rm gal}$). The filled symbols mark the seven galaxies. Right: the templates of stellar atmospheres from the Kurucz atlas are superimposed onto the observed SEDs of five out of the 11 star candidates fainter than $K_s > 21$.

& Pellò 2000) has been used to obtain the best-fitting templates. The set of templates used has been selected among a large grid of models to provide us with the most accurate estimate of the redshift for the galaxies in our photometric sample. The grid from which we selected the final set of templates, includes declining star formation rates (SFRs) with time-scale τ in the range 0.1–15 Gyr besides the Simple Stellar Population (SSP) and the Constant Star Formation (cst) models. The templates have been produced at solar metallicity with Salpeter, Scalo and Miller–Scalo initial mass functions (IMFs). Various ranges of extinction A_V and two different extinction laws (Prévot et al. 1984; Calzetti et al. 2000) have been considered in the best-fitting procedure.

The selection of the best set of templates has been performed by comparing the photometric redshifts z_p provided by the various sets of templates obtainable by the whole grid of models, with the spectroscopic redshifts z_s of a control sample of 232 galaxies. This sample includes 151 galaxies in the *Hubble Deep Field*-North (HDF-N; Cohen et al. 2000; Dawson et al. 2001; Fernández-Soto et al. 2002) and 81 in the HDF-S (Vanzella et al. 2002; Labbè et al. 2003b; Sawicki & Mallén-Ornelas 2003; Trujillo et al. 2004; Rigopoulou et al. 2005) with known spectroscopic redshift. The best set of templates is the one minimizing the mean and the standard deviation of the residuals defined as $\Delta z = (z_p - z_s)/(1 + z_s)$ and the number of outliers defined as those sources with $\Delta z > 4\sigma_{\Delta_z}$. Both mean and standard deviation are iteratively computed applying a 4σ clipping till the convergence. The final number of outliers includes all the galaxies removed by the clipping procedure.

The set of templates and the range of extinction providing the best results are summarized in Table 1. It is worth noting that the resulting best set does not include the SSP, contrary to some of the previous photometric redshift analysis. This is due to the fact that SSP templates always provide a better fit to the photometry then other star formation histories (SFHs) but a wrong redshift estimate, typically lower than the real one. This results both in a larger

Table 1. Parameters defining the best set of templates obtained by comparing the photometric redshift with the spectroscopic redshift of 232 galaxies, 151 in the HDF-N and 81 in the HDF-S.

Best set	
SFHs τ [Gyr]	0.1, 0.3, 1, 3, 15, cst
IMF	Miller–Scalo
Metallicity	$Z_\odot$
Extinction law	Calzetti (2000)
Extinction	$0 \leqslant E(B-V) \leqslant 0.3$

deviation of the residuals from the null value and in a larger scatter. In Fig. 5, the photometric redshifts obtained with the best set of templates are compared to the spectroscopic redshift of the 232 galaxies of our control sample. The typical scatter in our photometric redshift estimate is $\sigma_{\Delta z} = 0.065$ with a negligible deviation of the residuals from the null value ($\langle \Delta z \rangle = -0.015$). It can be seen from Fig. 5 that no correlation is present between the residuals and the redshift. We obtain three outliers (1 per cent) over the redshift range $0 < z < 6$, two of which (IDs 892 and 242) are in the HDF-S. Both these are well above the background on the I_{814}-band image while their surface brightness appears very faint in the K_s-band image. This fact could have implied a wrong estimate of the colours and, consequently, of the photometric redshift. However, looking at the spectrum of 892, we verified that its spectroscopic redshift is rather uncertain because it is based on a single emission line tentatively identified as Hα. It should be noted that both of them are fainter than $K_s = 23$, the magnitude at which we selected the complete sample to derive the LF (see Sections 4 and 5). In Table 2, we report the values of $\langle \Delta z \rangle$ and of $\sigma_{\Delta z}$ together with the number of outliers relevant to the spectroscopic samples in the HDF-N, HDF-S and whole sample for different redshift bins.

We verified the reliability of our photometric redshifts by comparing the spectroscopic and the photometric redshift distributions of the 232 galaxies. In Fig. 6, the cumulative distributions of the photometric and the spectroscopic redshift are shown. A Kolmogorov–Smirnov (K–S) test has provided a probability $P_{(KS)} \simeq 40$ per cent that the two distributions belong to the same parent population confirming the reliability of our estimate. The same result has been obtained considering separately the 151 galaxies in the HDF-N and the 81 in the HDF-S

3.2 Redshift and colour distributions

Once we defined the set of templates and parameters providing the most accurate estimate of the photometric redshift, we ran the χ^2 minimization procedure on the complete sample of 300 galaxies at $K_s \leqslant 23$. For those galaxies having a spectroscopic redshift (74 at $K_s \leqslant 23$), the best fit has been constrained to the observed value. In Fig. 7, the redshift distribution of the sample is shown. The distribution has a median redshift $z_m = 1.15$ and has a tail extending up to $z_p \simeq 6$. There are 14 galaxies with photometric redshift $z_p > 4$, five of which are at $5 < z_p \leqslant 6$. The $J_s - K_s$ colour of the 300 galaxies is shown in Fig. 8. Three of the $J_s - K_s > 3$ galaxies were noticed on shallower near-IR images (Saracco et al. 2001) and previously analysed resulting in high-mass evolved galaxies at $2 < z < 3$ (Saracco et al. 2004). In Fig. 8, we also plot the expected $J_s - K_s$ colour obtained in the case of $E(B-V) = 0$ assuming a declining SFR with time-scale $\tau = 1$ Gyr seen at 5, 2 and 0.5 Gyr (from the top, thick lines) and a cst seen at 1 Gyr (dot-dashed line). The 1-Gyr-old cst model is reddened by $E(B-V) = 0.5$ to account for dusty star-forming galaxies (dot-dashed line). Most of the galaxies lie within the region limited by the 5-Gyr-old model towards the red and by the 0.5-Gyr-old model towards the blue. The reddest galaxies of the sample (at $2 < z < 3$) can be described by old stellar populations, i.e. populations with an age comparable to the age of the Universe at the relevant

4 *K*-CORRECTIONS AND NEAR-IR LUMINOSITIES

The estimate of the *k*-correction and of the absolute magnitude in the near-IR rest frame is a critical step when dealing with

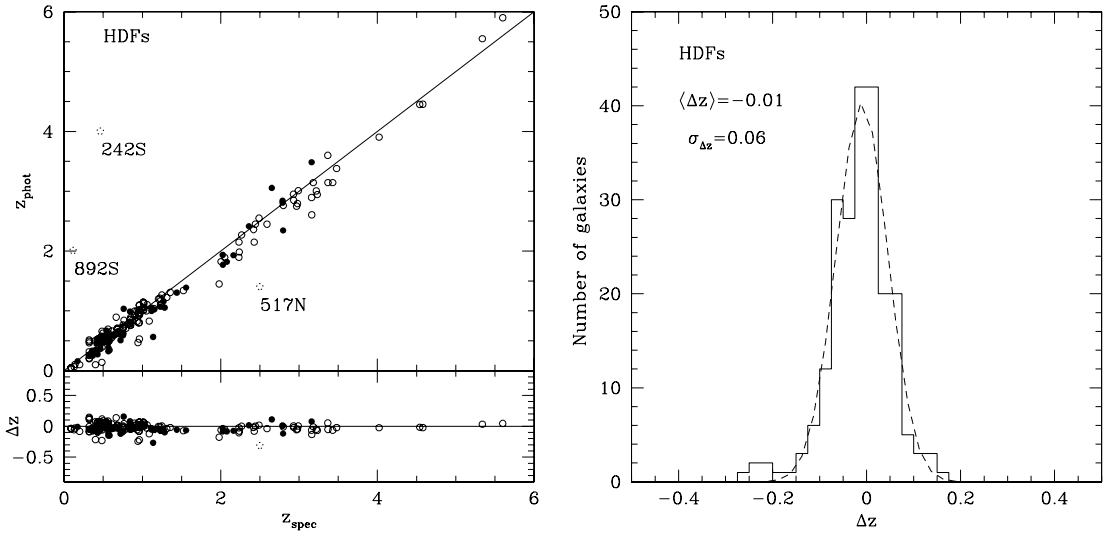

Figure 5. Left: comparison of photometric and spectroscopic redshifts for 232 galaxies (upper panel), 151 of which are in the HDF-N (empty circles) and 81 of which are in the HDF-S (filled circles). The outliers are marked by dotted circles. The numbers refer to the ID number in the Fernández-Soto et al. (2002) photometric catalogue for the HDF-N and to our photometric catalogue for the HDF-S. In the lower panel, the residuals Δz are plotted as a function of the spectroscopic redshifts. Right: distribution of the residuals Δz (histogram) for the whole spectroscopic sample. A Gaussian (dashed line) with $\sigma = 0.065$ and a mean deviation of $\langle \Delta z \rangle = -0.015$ from zero is superimposed onto the observed distribution.

Table 2. Mean and standard deviation of the residuals Δz for the spectroscopic samples of 232 galaxies (151 galaxies in the HDF-N and 81 in the HDF-S). For each estimate, the results obtained without and with the 4σ clipping are shown.

	$0 < z < 2$			$2 < z < 6$			$0 < z < 6$		
	$\Delta z \pm \sigma_{\Delta z}$	Outliers		$\Delta z \pm \sigma_{\Delta z}$	Outliers		$\Delta z \pm \sigma_{\Delta z}$	Outliers	
HDF-N	0.0 ± 0.066			-0.044 ± 0.068			-0.009 ± 0.068		
	0.0 ± 0.066	0/118		-0.044 ± 0.068	1/33	(3 per cent)	-0.007 ± 0.064	1/151	(<1 per cent)
HDF-S	0.033 ± 0.378			-0.017 ± 0.075			0.026 ± 0.353		
	0.033 ± 0.063	2/71	(3 per cent)	-0.017 ± 0.075	0/10		0.030 ± 0.065	2/81	(2 per cent)
HDFs	0.012 ± 0.230			-0.037 ± 0.070			0.002 ± 0.210		
	-0.011 ± 0.066	2/189	(1 per cent)	-0.037 ± 0.070	0/43		-0.015 ± 0.065	3/232	(1 per cent)

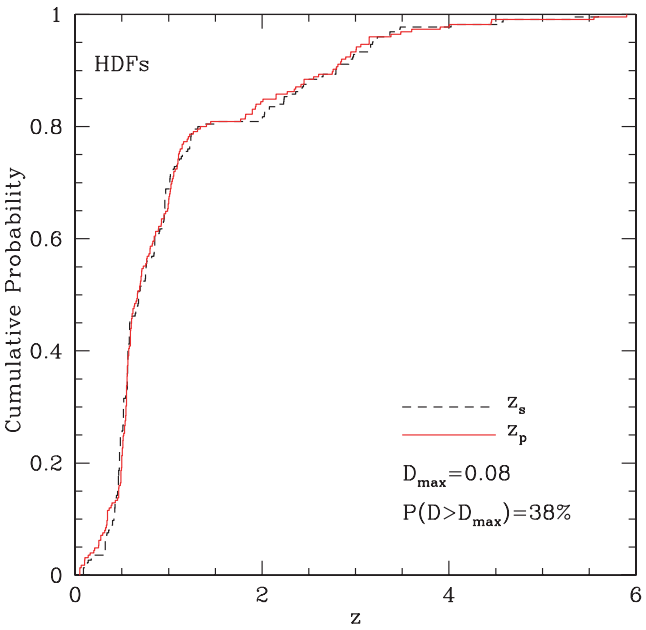

Figure 6. Cumulative distributions of photometric (continuous line) and spectroscopic (dashed line) redshift of the 232 galaxies with known redshift. The K–S test performed shows that the two distributions belong to the same parent population.

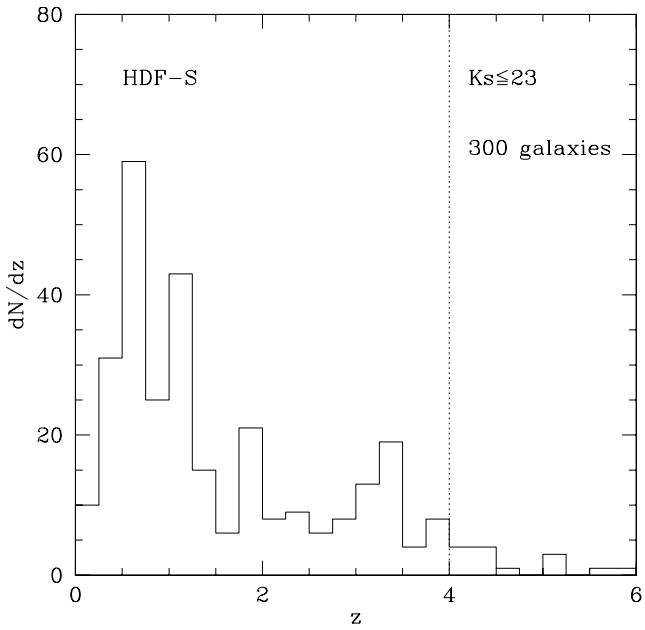

Figure 7. Redshift distribution of the complete sample of 300 galaxies brighter than $K_s = 23$ in the HDF-S. The median redshift is $z_p = 1.15$. The dotted line at $z_p = 4$ marks the redshift limit of the highest redshift bin considered in the LF estimate (see Section 5).

high-redshift galaxies. Indeed, unless we have photometry that is sampling the near-IR rest frame, an extrapolation with respect to the observed wavelength is required. This extrapolation is usually based on the best-fitting template, which should be a good approximation of the true (but unknown) SED of the galaxy. In fact, the larger the redshift, the wider the extrapolation and, possibly, the uncertainty affecting the rest-frame near-IR luminosity. Moreover, this estimate can also be affected by systematics due to the different libraries of models, which can differ substantially in the near-IR domain. We have tried to assess whether and how such uncertainties affect the estimate of the rest-frame near-IR luminosity. We first checked the robustness of the rest-frame near-IR luminosity with respect to the extrapolated photometry and then with respect to the different models. For each galaxy, we compared the rest-frame J_s-band absolute magnitude obtained from the equation

$$M_{J_s}(k_J) = J_s - 5\log[D_L(z)] - 25 - k_J(z), \quad (1)$$

where $D_L(z)$ is the luminosity distance at redshift z in units of Mpc, to the one derived by the equation

$$M_{J_s}(k_{JY}) = m_Y - 5\log[D_L(z)] - 25 - k_{JY}(z). \quad (2)$$

In equation (1), $k_J(z) = [J_{s,\rm rest} - J_s(z)]_{\rm temp}$ is the conventional k-correction obtained as the difference between the rest frame and observed magnitude computed on the best-fitting template. To this end, the transmission curve of the ISAAC-J_s filter has been multiplied with the best-fitting template at rest and redshifted to z (where $z = z_s$ for the 74 galaxies with known redshift in the K23 sample). In equation (2), $k_{JY} = [J_{s,\rm rest} - Y(z)]_{\rm temp}$ and m_Y is the observed apparent magnitude in the filter Y that best matches the rest-frame J_s band of the galaxy at the relevant redshift (e.g. Lilly et al. 1995a; Pozzetti et al. 2003). In our case $Y = J_s$, H, K_s according to the redshift of the galaxy. Both the 'colour k-correction' terms, $k_J(z)$ and k_{JY}, include the flux density dimming factor $(1 + z)$ independent of wavelength. In Fig. 9 (left panel), the difference between the rest-frame J_s-band absolute magnitude derived for each galaxy from equations (1) and (2) is plotted as a function of z. Up to $z \sim 2$, where the near-IR filters sample wavelengths $\lambda_{J_s} > 0.4\,\mu$m and $\lambda_{K_s} > 0.7\,\mu$m, the two equations provide the same values within an rms of about 0.15 mag, comparable to or lower than the typical

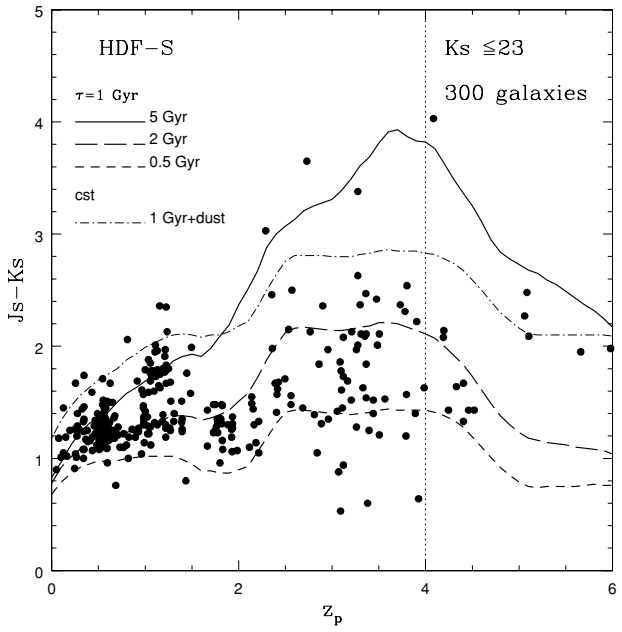

Figure 8. $J_s - K_s$ colour of galaxies versus redshift. The thick curves represent (from the top) the $J_s - K_s$ colour derived by a declining star formation rate ($e^{-t/\tau}$) with e-folding time $\tau = 1$ Gyr and $E(B - V) = 0$ seen at 5, 2 and 0.5 Gyr. The thin curve is a dusty ($A_V = 2$) constant star formation (cst) seen at 1 Gyr. The templates have been obtained with a Salpeter IMF at solar metallicity. The dotted line at $z = 4$ marks the redshift limit of the highest redshift bin considered in the LF estimate (see Section 5).

photometric error. This dispersion does not affect the estimate of the LF. This is shown in the right panel of Fig. 9 where the distributions of the rest-frame J_s-band absolute magnitude derived from equation (1) (solid histogram) and from equation (2) (dotted histogram) are compared for galaxies in different redshift bins. At $z < 2$, the two distributions belong to the same parent population as confirmed by the K–S test we performed. At larger redshift, the conventional equation (1) provides absolute magnitudes which can differ systematically from those derived from equation (2). These differences can bias the estimate of the LF. The absolute magnitude distributions shown in Fig. 9 for galaxies at $z > 2$ are indeed rather different, even if the difference is only marginally significant. Thus, until the near-IR band chosen to construct the LF (the J_s filter in our example) samples the part of the SED redwards of $\lambda > 0.4$ μm, characterized by a regular shape, dominated by the emission of older stars and weakly affected by dust extinction and star formation, equations (1) and (2) provide consistent absolute magnitudes. In this case, having photometry approaching the rest-frame wavelength of the chosen filter (the K_s band in our example) and using equation (2) do not improve the accuracy and the reliability of the estimate of the LF. In contrast, when the chosen near-IR filter samples the blue and UV part of the spectrum ($\lambda_{J_s} < 0.4$ μm at $z > 2$), the observed emission in that filter (J_s) is dominated by young ($K_s < 0.5$ Gyr) stars which do not contribute significantly to the red part of the spectrum, i.e. to the rest-frame luminosity we want to derive. Moreover, it can be strongly affected by dust extinction. In this case, the extrapolation to the near-IR rest-frame wavelength required by equation (1) can give wrong values and the photometry in the redder band, the K_s filter in our case, is needed to apply equation (2).

We then checked the dependence of the LF on the different library of models used to derive the best-fitting template. Recently, Maraston (2005; M05 hereafter) has shown the importance of the thermally pulsing asymptotic giant branch (TP-AGB) phase in modelling young stellar populations. This evolutionary phase can play an important role in the continuum emission of a stellar population at $\lambda > 0.4$–0.5 μm with ages younger than 1 Gyr. The modelling of this phase in the Maraston code produces a brightening in the near-IR with respect to the same stellar populations (equal age, IMF and metallicity) modelled by the BC03 and PEGASE (Fioc & Rocca-Volmerange 1997) codes. To assess whether this difference affects the estimate of the LF, we compared the distributions of the K_s-band absolute magnitudes obtained with the BC03 and M05 models. We did not include the PEGASE models in this comparison because they provide SEDs very similar to those of BC03.

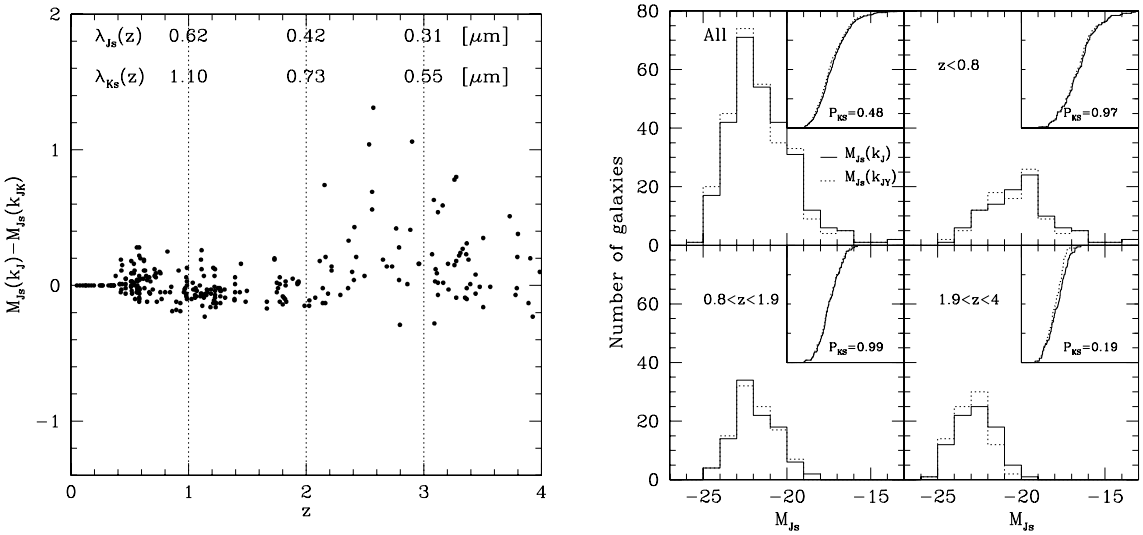

Figure 9. Left: the difference between the rest-frame J_s-band absolute magnitude derived for each galaxy from equations (1) and (2) is plotted as a function of z. Right: the distribution of the J_s-band absolute magnitude of galaxies derived from equation (1) (solid histogram) are compared to the one derived from equation (2) (dotted histogram) for different redshift bin. No significant differences are present between the distributions at $z < 2$ as confirmed by the high probability provided by the K–S test (small subpanels).

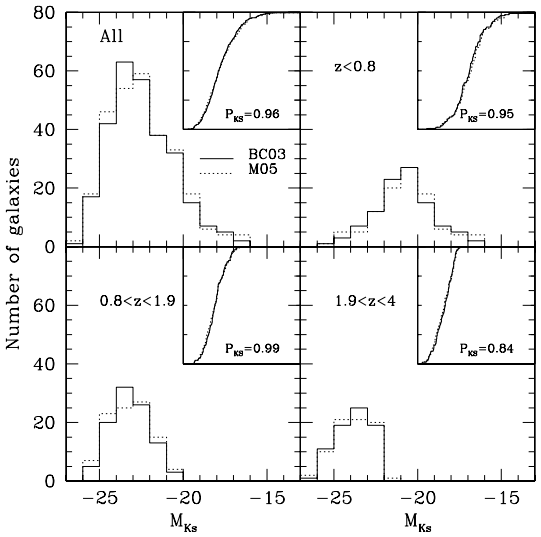

Figure 10. The K-band absolute magnitudes obtained with the Bruzual & Charlot (2003; BC03) models (solid histogram) for the sample of 285 galaxies at $z < 4$ are compared with those obtained with the Maraston (2005; M05) models (dotted histogram) for different redshift bins. The distributions belong to the same parent population as shown by the high probability provided by the K–S test we performed (small panels).

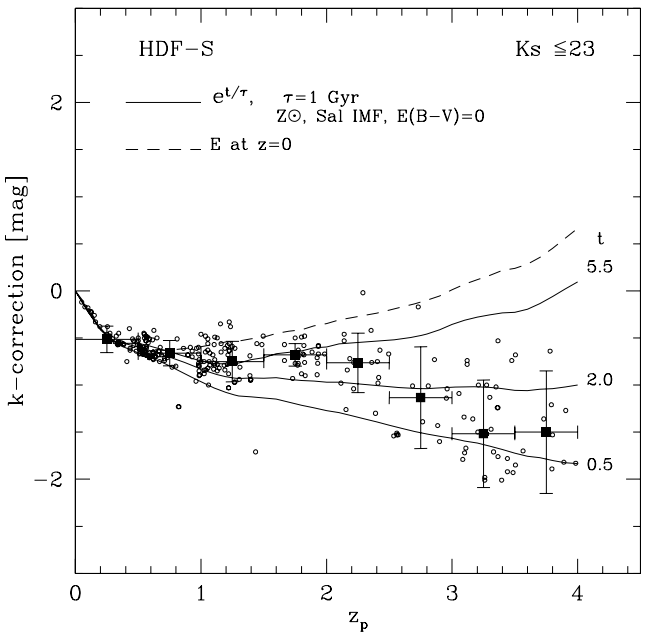

Figure 11. K_s-band k-correction as a function of redshift for the 285 galaxies brighter than $K_s = 23$ at $z \leqslant 4$ in the HDF-S (small open circles). The filled squares are the median values of the k-correction in redshift bins 0.5 width (horizontal error bars). The error bars along the y-axis represent the scatter within each bin. The continuous lines are the k-corrections derived by a model described by an exponentially declining star formation rate with $\tau = 1$ Gyr and t (from top) 5, 2 and 0.5 Gyr. The dashed line represent the k-correction of local ellipticals derived by the mean observed spectrum of ellipticals (Mannucci et al. 2001).

We constructed the same set of templates described in Table 1 using the SSPs of M05 and, for each galaxy, we searched for the best-fitting template at the relevant redshift. In Fig. 10, the absolute magnitude distributions obtained with the two sets of models for the whole sample of galaxies at $z < 4$ and in three redshift bins are shown. The K–S test we performed does not show evidence of a difference between the distributions providing probabilities $P(\mathrm{KS}) > 0.8$ in all the redshift bins.

The above results show that our study of the LF and of its evolution with redshift is not dependent either on the method used to derive the rest-frame absolute magnitudes or on the library of templates used at least down to $z \simeq 2$. Therefore, we are confident of the reliability of our estimate of the LF at least down to this redshift. However, we chose to push our study of the LF at $z < 4$ because the K_s band still samples the red part ($\lambda_{K_s} > 0.45$ μm) of the SED down to this redshift limit. We will use equation (2) to derive the rest-frame J_s-band absolute magnitudes and the conventional form of equation (1) to compute the K_s-band absolute magnitudes. In Fig. 11, the K_s-band k-correction derived for the sample of 285 galaxies at $z < 4$ is shown as a function of redshift. For comparison, superimposed on the data, we plot the k-correction as derived by three synthetic templates (continuous lines) obtained with a declining SFR seen at three different ages, (from the top) 5, 2 and 0.5 Gyr. Besides the models, we also plot (dashed line) the k-correction derived by the mean observed spectrum of local elliptical galaxies (Mannucci et al. 2001).

5 THE NEAR-IR LUMINOSITY FUNCTION IN THE HDF-S

5.1 Computing the LF with the $1/V_{\mathrm{max}}$ method

We computed the LF, $\Phi(M)\ \mathrm{d}M$, using the non-parametric $1/V_{\mathrm{max}}$ method (Schmidt 1968). This method does not require any assumption on the form of the LF and provides an unbiased estimate if the sample is not affected by strong density inhomogeneities. Previous studies of the LF of galaxies in the HDFs obtained with different estimators, both parametric and non-parametric (Takeuchi, Yoshikawa & Ishii 2000; Bolzonella et al. 2002), show no differences with respect to the LF obtained with the V_{max} formalism. This implies that no strong inhomogeneities are present in the HDF-S and that our results are not dependent on the LF estimator used. In the $1/V_{\mathrm{max}}$ method, given a redshift bin $[z_l, z_u)$, each galaxy contributes to the number density of galaxies in that bin an amount inversely proportional to the maximum volume:

$$V_{\mathrm{max},i} = \int_{\Omega}\int_{z_l}^{\min(z_u, z_{\mathrm{max},i})} \frac{\mathrm{d}^2 V}{\mathrm{d}z\,\mathrm{d}\Omega}\,\mathrm{d}z\,\mathrm{d}\Omega, \tag{3}$$

where $z_{\mathrm{max},i}$ is the maximum redshift at which the galaxy i with absolute magnitude $M_i \in [M, M + \mathrm{d}M]$ is still detectable given the limiting apparent magnitude $K_s = 23$ of the sample, $\mathrm{d}^2V/\mathrm{d}z\,\mathrm{d}\Omega$ is the comoving volume element and Ω is the solid angle covered by the surveyed area. In our case, the sample has been selected over an area of about 5.5 arcmin^2 of the HDF-S corresponding to a solid angle $\Omega \simeq 4.65 \times 10^{-7}$ sr. The comoving number density of galaxies $\Phi(M)\ \mathrm{d}M$ for each absolute magnitude bin in a given redshift bin and its error σ_Φ are computed as

$$\Phi(M)\,\mathrm{d}M = \sum_i \frac{1}{V_{\mathrm{max},i}}\,\mathrm{d}M$$

and (4)

$$\sigma_\Phi = \sqrt{\sum_i \left(\frac{1}{V_{\mathrm{max},i}}\right)^2}.$$

We defined the different redshift bins so that a comparable and statistically significant number of galaxies falls in each of them.

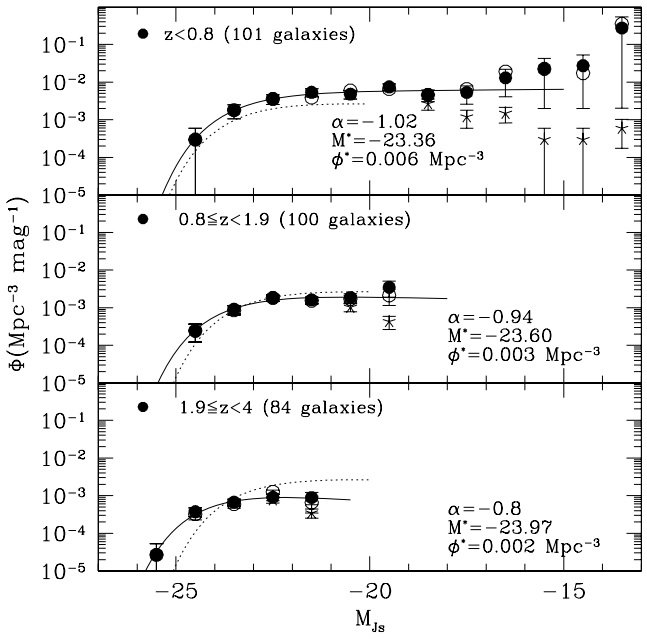

Figure 12. Rest-frame J_s-band luminosity function of galaxies derived with the $1/V_{max}$ method (circles) in the three redshift bins considered: $0 < z < 0.8$ ($z_m = 0.55$; upper panel), $0.8 \leqslant z < 1.9$ ($z_m = 1.2$; middle panel) and $1.9 \leqslant z < 4$ ($z_m = 3.1$; lower panel). We marked with open circles the LF obtained with the J_s-band luminosities derived from equation (1). The starred symbols show the LF uncorrected for the V_{max}. The faint end $M_{J_s} > -17$ of the LF is defined by nine galaxies at $z < 0.3$. Superimposed onto the LF is shown the formal fit obtained with a Schechter function (thin line). The dotted line is the local LF of Cole et al. (2001).

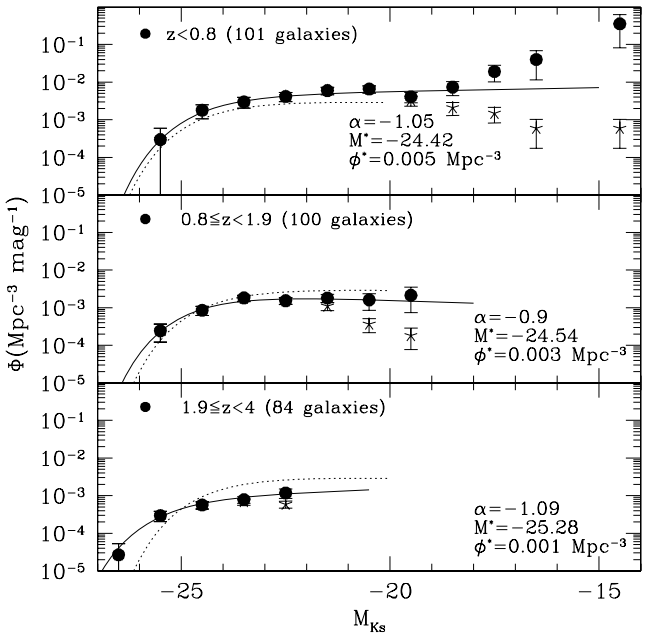

Figure 13. Rest-frame K_s-band luminosity function of galaxies and the Schechter best fit. Symbols are as in Fig. 12.

According to this criterion and to the results obtained in Section 4, we divided the sample of 285 galaxies at $z < 4$ into the three redshift bins [0; 0.8), [0.8; 1.9) and [1.9; 4). Each bin includes 101, 100 and 84 galaxies of which there are 52 (50 per cent), 12 (12 per cent) and 10 (12 per cent) with spectroscopic redshift, respectively. The median redshifts in the three bins are $z_m = 0.55$, 1.2 and 3.1, respectively.

The rest-frame J_s- and K_s-band LFs we derived in each redshift bin are shown in Figs 12 and 13 respectively (filled points). The starred symbols denote the LF uncorrected for the incompleteness and show where the $1/V_{max}$ correction takes place. In Fig. 12, the J_s-band LF obtained with the rest-frame J_s-band absolute magnitudes derived from equation (1) is also shown (empty points). The figures suggest a systematic decrease of the number density of bright galaxies coupled with a systematic brightening of the LF going to high redshift. This trend is present both in the J_s- and K_s-band LFs. We will probe further these features in the next section. Besides this, the figures are also suggestive of a raise of the LF at faint absolute magnitudes ($M_{J_s} > -17$ and $M_{K_s} > -18$) in the lowest redshift bin: a rise that cannot be probed in the two bins at higher redshift where brighter galaxies are selectively missed. The same slope of the faint end is obtained by computing the LF in the redshift range $0 < z < 0.4$ suggesting that the rise is not due to possible exceeding values of $1/V_{max}$. However, it is worth noting that the rise we see is based on very low statistics. Indeed, the faint end is defined by nine out of the 12 galaxies at $0.1 < z < 0.3$ in our sample. It is indeed expected that, given the criterion adopted to select the HDF-S (devoid of bright sources), galaxies at low redshift in this field are low-luminosity galaxies ($M_K > -20$). This, coupled with the very faint limit ($K_s = 23$) of the sample, allows to probe the faint end of the LF at $\langle z \rangle \simeq 0.2$ down to the unprecedented faint near-IR magnitude $M \simeq -14$. These low-luminosity galaxies are slightly bluer in the optical ($0.45 < V_{606} - I_{814} < 0.9$) than the bulk of the galaxies in the HDF-S, while their optical-IR colours ($1.4 < I_{814} - K_s < 2.7$, $0.9 < J_s - K_s < 1.5$) are consistent with those of the bulk. All but one are brighter than $V = 25.8$ and $I = 24.9$ and are in the range $21 < K_s < 22.9$. Most of them show an irregular morphology, while two of them appear very compact. In Fig. 14, the V_{606}- (upper panels) and I_{814}-band (lower panels) images of seven out of the nine galaxies at $z < 0.3$ fainter than $M_K = -18$ are shown. Both the apparent rise of the LF at faint luminosities and the irregular morphology of the galaxies populating the faint end are consistent with previous estimates of the local LF of galaxies at optical wavelengths. Such estimates show that the faint end of the near-IR LF is dominated by irregular and dwarf galaxies whose contribution to the comoving number density increases going to lower luminosities as found for the local LF in the optical rest frame (e.g. Marzke et al. 1994, 1998; Zucca et al. 1997; Folkes et al. 1999). We estimated a comoving number density of galaxies with magnitude $-19 < M_K < -14$ of $\bar{n}_{faint} = 0.4 \pm 0.27\,Mpc^{-3}$ at $\langle z \rangle \simeq 0.2$. This value agrees with the one derived locally by Zucca et al. (1997) for galaxies $M_{b_J} > -17$ and it is nearly 1 order of magnitude higher than the comoving density of brighter galaxies ($\bar{n}_{bright} = 0.039 \pm 0.005\,Mpc^{-3}$ for $M_K < -19$). However, the very low statistic, the uncertainty in the photometric redshift estimate and the small volume sampled by the HDF-S, especially at low redshift, prevent us from strongly constraining the faint end of the LF. The possible rise we see at very faint near-IR luminosities needs a larger sample to be established.

5.2 The evolution of the LF of galaxies in the HDF-S

In Figs 12 and 13, we plot the formal fitting to the LFs we obtained with a Schechter function (Schechter 1976). The fitting is performed over the whole range of absolute magnitudes spanned by the LFs in each redshift bin. The results of the fitting are summarized in Table 3 where we report the values of the parameters α, M^* and ϕ^* in each redshift bin. In Fig. 15, the errors contours at the 68 per

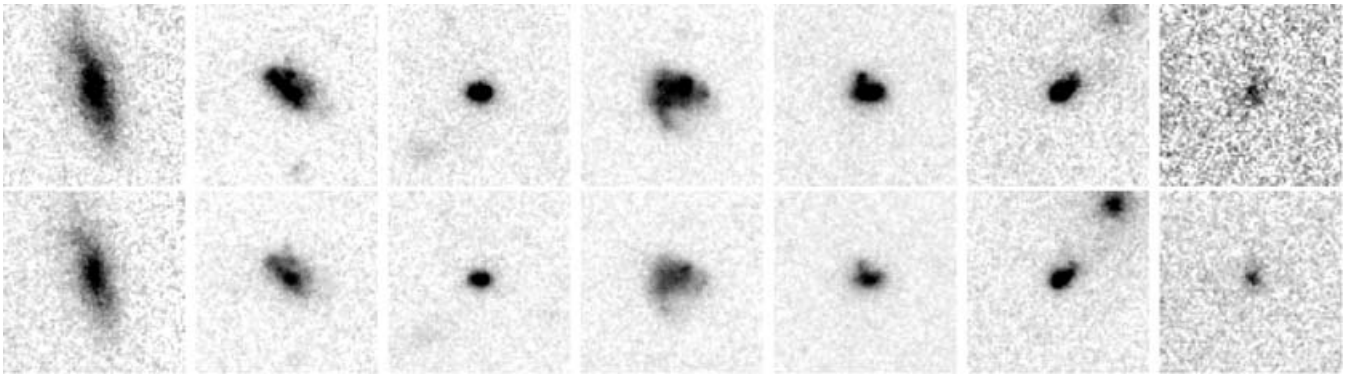

Figure 14. V_{606}-band (upper panels) and I_{814}-band (lower panel) images of seven out of the nine galaxies at $z < 0.3$ fainter than $M_K = -19$ galaxies. The images are 3 × 3 arcsec centred on the source. The intensity of the images are optimized to show the galaxies. Galaxies are displayed from left to right on the basis of their V_{606}-band apparent magnitude.

Table 3. Parameters α, M^* and ϕ^* of the Schechter function obtained by fitting the J_s- and K_s-band LFs in the three redshift bins.

z-bin	α	M^*	ϕ^* (10^{-3} Mpc^{-3})
		J_s band	
0.0–0.8	$-1.02^{+0.10}_{-0.10}$	$-23.36^{+0.63}_{-0.57}$	$6.0^{+2.3}_{-1.6}$
0.8–1.9	$-0.94^{+0.16}_{-0.15}$	$-23.60^{+0.35}_{-0.36}$	$2.6^{+1.1}_{-1.0}$
1.9–4.0	$-0.81^{+0.34}_{-0.25}$	$-23.97^{+0.50}_{-0.52}$	$2.0^{+0.8}_{-0.6}$
		K_s band	
0.0–0.8	$-1.05^{+0.11}_{-0.10}$	$-24.42^{+0.65}_{-0.58}$	$5.2^{+2.4}_{-1.5}$
0.8–1.9	$-0.90^{+0.18}_{-0.15}$	$-24.54^{+0.35}_{-0.38}$	$2.8^{+1.1}_{-0.9}$
1.9–4.0	$-1.09^{+0.34}_{-0.27}$	$-25.28^{+0.52}_{-0.54}$	$1.0^{+0.7}_{-0.5}$

cent confidence level for the joint parameters [α, M^*] and [ϕ^*, M^*] of the K_s-band LF fit are shown. The decreasing number density and the possible brightening previously noticed in the LFs going to high redshift are evident in the plot. However, given the statistical correlation between the Schechter parameters (α, M^* and ϕ^*), we will probe further on the significance of this evolution by fixing the α parameter. Fig. 15 suggests also that we cannot constrain the faint end of the LF and thus the parameter α at high redshift. However, we tried to constrain the evolution of the LF shape by means of the K–S test (see e.g. Feulner et al. 2003), which uses all the absolute magnitudes without binning. We derived in each redshift bin the cumulative LF (CLF) which gives the number of galaxies per unit volume brighter than M. In the upper panel of Fig. 16, we show the three CLFs obtained in the K_s band. Because the K–S test compares the CLFs normalized to unity, this test is not able to detect variations of ϕ^*. The normalized CLFs provide information on the relevant distribution of galaxies within the range of absolute magnitudes considered, i.e. on the form of the LF. For this reason, we expect that the K–S test is more sensitive to the variation of α which defines the form of the distribution rather than of M^*.

To quantify the sensitivity of the K–S test to the variations of α and M^* for samples of the same size as our sample, we simulated and compared among them various samples of 100 objects described by a Schechter LF with different values of α and M^*. We have found that, at the 90 per cent confidence level, the minimum variations we are able to detect on α and M^* on our samples are ± 0.3 and ± 0.8 mag, respectively. In the lower panel of Fig. 16, the normalized CLFs obtained in the three redshift bins are compared two by two [lowest- versus mid-redshift bin (upper panel) and mid- versus highest-redshift bin (lower panel)]. The K–S test does not point out significant differences among the distributions as shown by the probabilities $P_{KS} \simeq 0.61$ (bin 1 versus bin 2) and $P_{KS} \simeq$

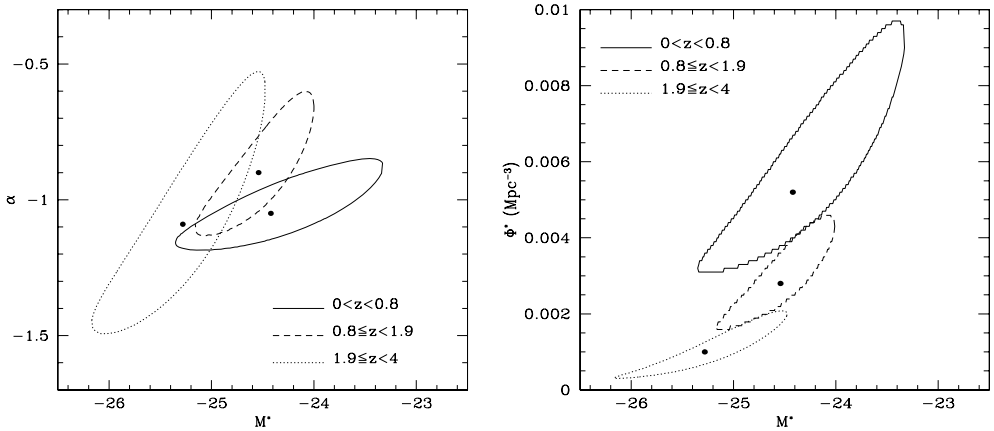

Figure 15. Error contours at the 68 per cent confidence level for the parameters [α, M^*] (left panel) and [ϕ^*, M^*] (right panel) of the K_s-band Schechter fit of Fig. 13.

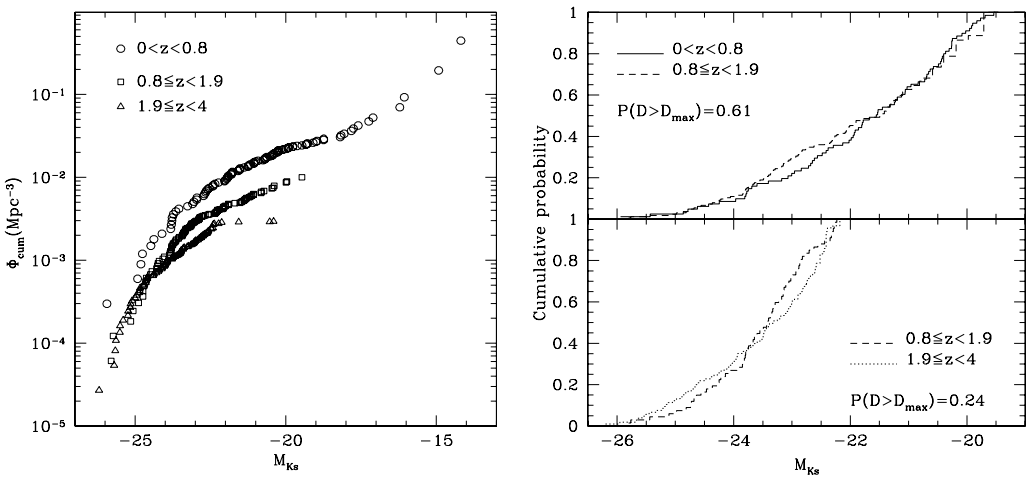

Figure 16. Left: cumulative luminosity function of galaxies derived with the $1/V_{\rm max}$ in the three redshift bins: $0 < z < 0.8$ (circles), $0.8 \leqslant z < 1.9$ (squares) and $1.9 \leqslant z < 4$ (triangles). Right: two-by-two comparison of the cumulative LFs in the three redshift bins normalized over the range of absolute magnitudes in common.

0.24 (bin 2 versus bin 3). Thus, we conclude that, if α changes, its variation has to be lower than 0.3 from $z_{\rm m} \simeq 0.6$ to 3.

We then probed the evolution of M^* and ϕ^* by comparing the values obtained by fitting a Schechter function for a fixed value of α. We assumed the value $\alpha = -1.0$ because it is very close to the values we derived in each redshift bin and to the values previously derived by other authors for local galaxies (e.g. Loveday 2000; Kochanek et al. 2001). The results of the fitting are summarized in Table 4 and shown in Fig. 17. The possible brightening combined with the decreasing number density of bright galaxies previously noticed in the LF from $z_{\rm m} \simeq 0.6$ to 1.2 is confirmed and, possibly, it extends to $z_{\rm m} \sim 3$. The normalization of the LF and, consequently, the number density of bright galaxies decreases by a factor 3 from $z_{\rm m} \simeq 0.6$ to 1.2. In parallel, the characteristic magnitude M^* brightens by $\sim$0.4 mag. The evolution of ϕ^* is detected at a high confidence level ($>3\sigma$), as shown by the error contours shown in Fig. 18, while the significance of the brightening of M^* is 1σ. The same trend persists, even if at a low confidence level for $\phi^*(<2\sigma)$, from $z_{\rm m} \simeq 1.2$ to 3 where $\phi^*(z \sim 3) \simeq 0.5\phi^*(z \sim 1.2)$ and M^* brightens by $\sim$0.4 mag. It is worth noting that this evolution is not dependent on the value assumed for α. Indeed, by assuming $\alpha = -1.1$, we obtain for the $K_{\rm s}$-band LF fit $M^*(z \sim 0.6) = -24.62$ and $\phi^*(z \sim 0.6) = 0.0045$ Mpc^{-3} to be compared with $M^*(z \sim 1.2) = -25.03$ and $\phi^*(z \sim 1.2) = 0.0016$ Mpc^{-3}, resulting in the same luminosity and density evolution (see Table 4).

Table 4. Parameters M^* and ϕ^* of the Schechter function fitting the $J_{\rm s}$- and $K_{\rm s}$-band LFs with $\alpha = -1.0$ and the $K_{\rm s}$-band LF with $\alpha = -1.1$. to the LF in the three redshift bins.

z-bin	ΔM	M^*	ϕ^* (10^{-3} Mpc^{-3})
	$J_{\rm s}$	$\alpha = -1.0$	
0.0–0.8	−25;−17	$-23.30^{+0.40}_{-0.40}$	$6.5^{+1.0}_{-0.9}$
0.8–1.9	−25;−19	$-23.72^{+0.22}_{-0.22}$	$2.2^{+0.2}_{-0.2}$
1.9–4.0	−26;−21	$-24.20^{+0.21}_{-0.20}$	$1.2^{+0.2}_{-0.2}$
	$K_{\rm s}$	$\alpha = -1.0$	
0.0–0.8	−26;−18	$-24.32^{+0.41}_{-0.40}$	$6.3^{+1.1}_{-1.0}$
0.8–1.9	−26;−19	$-24.76^{+0.23}_{-0.23}$	$2.1^{+0.2}_{-0.3}$
1.9–4.0	−27;−22	$-25.15^{+0.25}_{-0.23}$	$1.1^{+0.2}_{-0.2}$
	$K_{\rm s}$	$\alpha = -1.1$	
0.0–0.8	−26;−19	$-24.62^{+0.40}_{-0.39}$	$4.5^{+1.1}_{-1.0}$
0.8–1.9	−26;−19	$-25.03^{+0.22}_{-0.21}$	$1.6^{+0.2}_{-0.3}$
1.9–4.0	−27;−22	$-25.28^{+0.23}_{-0.20}$	$0.9^{+0.2}_{-0.2}$

6 THE EVOLUTION OF THE NEAR-IR LF TO $z \sim 3$

In this section, we compare our results with those obtained by other authors both at lower and at comparable redshift in order to constrain the evolution of the near-IR LF of galaxies from $z \sim 3$ to 0.

6.1 The $K_{\rm s}$-band LF

In Table 5, the parameters of the Schechter function of the $K_{\rm s}$-band LF obtained by various authors with different samples are summarized. In Fig. 19, the fitting Schechter functions obtained by the various authors are shown in the range of absolute magnitudes reached by the surveys according to the values reported in Table 5 [M_K(min)]. We first compared the $K_{\rm s}$-band LF we derived at $z_{\rm m} \simeq 0.6$ with those derived on local samples of galaxies in order to probe and constrain the evolution of the LF in the last 4 Gyr. In particular, we considered the LFs of Cole et al. (2001), Kochanek et al. (2001) and that of Loveday (2000). These three local LFs are consistent among them. The former two are based on the largest samples of local galaxies, while the latter extends down to very faint luminosities [M_K(min) $\simeq -16$]. In Fig. 19, the three local LFs are superimposed onto the LF we derived at $z_{\rm m} \simeq 0.6$ (left upper panel) based on 101 galaxies 50 per cent of which have spectroscopic redshift. The agreement with the LFs of Kochanek et al. and of Loveday et al. is rather good. The largest deviation is with respect to the LF of Cole et al. However, this deviation is not significant as is also confirmed by the K–S test, which gives $P_{\rm KS} \simeq 0.5$. The characteristic magnitude of the Schechter function we derive at $z_{\rm m} \sim 0.6$ is consistent, although

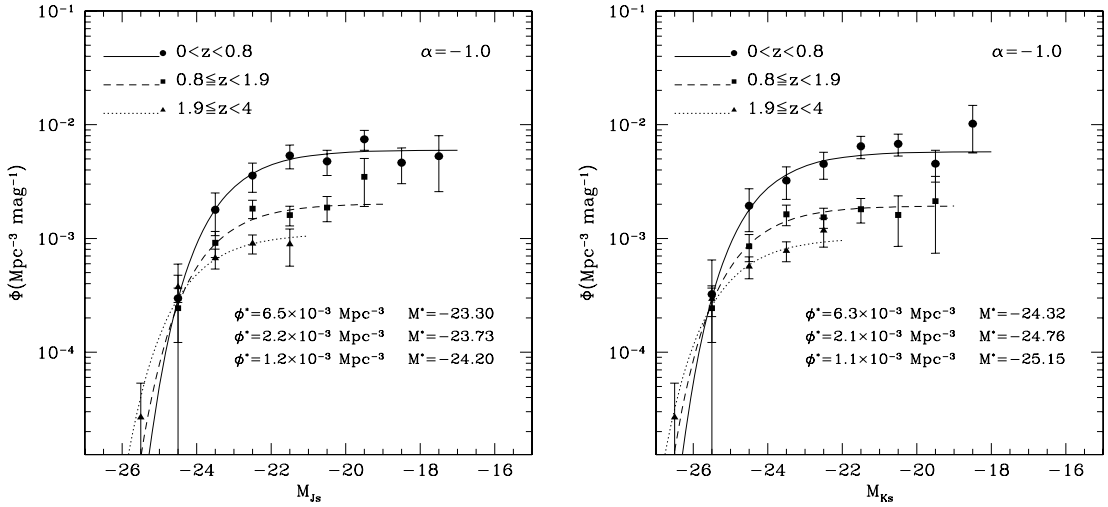

Figure 17. Left: superimposed on the J_s-band LFs are shown the relevant best fits obtained with a Schechter function with $\alpha = -1.0$. Right: the same as in the left panel but for the K_s band.

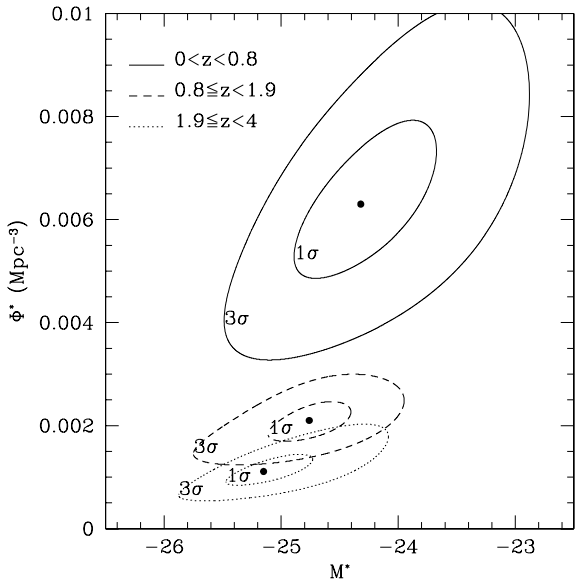

Figure 18. Error contours at 1σ and 3σ for the parameters ϕ^* and M^* of the Schechter fit with $\alpha = -1.0$ to the K_s-band LF.

brighter by about 0.2–0.3 mag, with the local values (see Table 5). No differences are found between the value of ϕ^* we estimate at $z \sim 0.6$ and the local values. Thus, the comparison with the local near-IR LF of galaxies does not point out evidence of strong luminosity and/or density evolution at $z < 0.8$. Given the statistical errors of our estimate, we conclude that the near-IR LF has evolved not more than 0.2–0.3 mag in the last 4 Gyr.

We then compared our LF at $z_m \sim 0.6$ with those derived at comparable redshift. In the right upper panel of Fig. 19, the Schechter functions representing the LFs obtained by Glazebrook et al. (1995), Feulner et al. (2003), Bolzonella et al. (2002) and Pozzetti et al. (2003) at $z \sim 0.5$ are superimposed onto our estimate. Glazebrook et al. and Feulner et al. derive the LF assuming a value of α of -1.0 and -1.1, respectively. The LF we obtained with these values of α, summarized in Table 4, are in very good agreement with the results of Glazebrook et al. and Feulner et al. The largest deviations are with respect to the LF of Bolzonella et al. and of Pozzetti et al. Both these LFs are characterized by steeper values of α and brighter characteristic magnitudes with respect both to our and the other LFs at these and lower redshifts. The K–S test we performed shows that the deviation from the LF of Pozzetti et al. is not significant ($P_{KS} \simeq 0.15$), while the deviation from the LF of Bolzonella et al. is significant ($P_{KS} \simeq 0.02$). This latter result, rather surprising because we deal with the same field, is also evident by comparing the LF we obtained at higher redshift. In the lower left panel of Fig. 19, the LFs obtained by Pozzetti et al. at $0.75 < z < 1.3$, by Kashikawa et al. (2003) at $1 < z < 1.5$ and by Bolzonella et al. at $1 < z < 2$ are superimposed onto the one we obtained in the redshift range $0.8 \leqslant z < 1.9$. The agreement with the LF of Pozzetti et al. is remarkable. In contrast, it is evident that our LF is not consistent with the LFs of Bolzonella et al. and of Kashikawa et al. who find a very steep ($\alpha < -1.35$) LF coupled with a very bright ($M*_K < -25.5$) characteristic magnitude. In both cases, the K–S test gives a probability of less than 1 per cent that the distributions are drawn from the same parent population. This is shown in Fig. 20 where the cumulative distributions relevant to these LFs are shown. The reasons for this disagreement have to be searched both in the different samples and magnitudes used by Bolzonella et al. and Kashikawa et al.

As to the LF of Bolzonella et al., even if relevant to the HDF-S, it is based on a near-IR sample extracted from an optically selected catalogue (Vanzella et al. 2001). At variance with respect to our sample, detection and magnitude estimates were performed and optimized on optical *HST* images. Moreover, the selection and completeness of the near-IR sample extracted by Bolzonella et al. are based on the $I_{814} - K_s$ colour distribution. The near-IR data are 4 times shallower than those used in the present work and, consequently, the sample is $\sim$1 mag shallower. It should also be noted that 25 per cent of our sample (50 per cent of the sample at $z < 0.8$) has spectroscopic redshift and that these redshifts have been used both to optimize the photometric redshift and to estimate the LF. All that implies differences in the near-IR magnitude estimates which can account for the different LF obtained.

As to the comparison with the LF of Kashikawa et al., no obvious reasons can be put forward for the disagreement we obtained in

Table 5. Summary of the parameters of the Schechter function obtained by various authors by fitting the K-band LF of different samples of field galaxies. For each sample, the relevant limiting magnitude, the area, the range of redshift covered by the survey (or the mean redshift of the sample) and the number of objects are reported. The parameters of the Schechter function and the faintest absolute magnitude sampled by the data are scaled to the cosmology adopted here ($\Omega_m = 0.3$, $\Omega_\Lambda = 0.7$, $H_0 = 70$ km s^{-1} Mpc^{-1}).

Source	m_{lim}	Area (arcmin^2)	z	No. of objects	M^*	α	ϕ^* 10^{-3} (Mpc^{-3})	M_K(min)
Mobasher, Sharples & Ellis (1993)[a]	$K \leqslant 13$ $B_J \leqslant 17$		0–0.1	181	-24.14 ± 0.30	-1.00 ± 0.30	3.8 ± 0.6	-22
Glazebrook et al. (1995)	$K \leqslant 17.3$	552	0–0.2	55	-23.91 ± 0.23	-1.04 ± 0.30	7.6 ± 1.8	-22
			0–0.8	124	-24.42 ± 0.11	-1.00	4.1 ± 0.4	-23.5
Cowie et al. (1996)	$K \leqslant 20$	26.2	0–1	393	-24.27	-1.25	1.0	-21
Gardner et al. (1997)	K$\leqslant$15	15 840	$\langle 0.14 \rangle$	465	-24.07 ± 0.17	-0.91 ± 0.24	4.9 ± 0.7	-21.5
Szokoly et al. (1998)	$K \leqslant 16.5$	2160	0–0.4	175	-24.57 ± 0.30	-1.30 ± 0.20	3.9 ± 1.0	-21.5
Loveday (2000)[a]	$b_J \leqslant 17.15$		$\langle 0.05 \rangle$	345	-24.35 ± 0.42	-1.16 ± 0.19	4.1 ± 0.3	-16
Kochanek et al. (2001)	$K \leqslant 11.25$	$<2.5 \times 10^7$	$\langle 0.02 \rangle$	3878	-24.16 ± 0.05	-1.09 ± 0.06	4.0 ± 0.3	-21
Cole et al. (2001)	$K \leqslant 13$	2.2×10^6	$\langle 0.05 \rangle$	17 173	-24.21 ± 0.03	-0.96 ± 0.05	3.7 ± 0.6	-20
Feulner et al. (2003)	$K \leqslant 17.5$	649	0.1–0.3	157	-24.56 ± 0.24	-1.10	3.8 ± 0.4	-21
			0.3–0.6	145	-24.81 ± 0.26	-1.10	2.4 ± 0.9	-23.5
Huang et al. (2003)	$K \leqslant 15$	1056	$\langle 0.14 \rangle$		-24.47 ± 0.08	-1.39 ± 0.09	4.5 ± 0.7	-20.5
Pozzetti et al. (2003)	$K \leqslant 20$	52	0.2–0.65	132	-24.87 ± 0.63	-1.25 ± 0.22	1.8 ± 1.2	-19.5
			0.75–1.30	170	-24.77 ± 0.49	-0.98 ± 0.45	2.9 ± 1.4	-23
Drory et al. (2003)[b]	$K \leqslant 19.5$	998	0.4–1.2	$\sim$5000				-23.5
Bolzonella et al. (2002)[c]	$K \leqslant 22$		0–1		-25.03 ± 0.28	-1.17 ± 0.09	3.4 ± 1.2	-17
			1–2		-25.71 ± 1.14	-1.42 ± 0.10	0.8 ± 0.7	-20.5
Caputi et al. (2005)[b]	$K \leqslant 22$	50	0–2.5	1600				
Kashikawa et al. (2003)[b]	$K \leqslant 24$	$\sim$4	0.6–1	439	-25.41 ± 0.20	-1.35 ± 0.04	2.3 ± 0.7	-18.5
			1–1.5		-25.53 ± 0.27	-1.35 ± 0.06	1.9 ± 0.8	-19.5
			1.5–2.5		-25.58 ± 0.12	-1.37 ± 0.05	1.3 ± 0.5	-19.5
			2.5–3.5		-24.66 ± 0.23	-1.70 ± 0.11	1.0 ± 0.7	-20
This work[b]	$K \leqslant 23$	5.5	0–0.8	101	-24.47 ± 0.63	-1.14 ± 0.11	4.0 ± 2.0	-14
			0.8–1.9	100	-24.53 ± 0.37	-0.85 ± 0.17	2.9 ± 1.0	-19
			1.9–4	84	-25.18 ± 0.53	-1.10 ± 0.31	1.0 ± 0.6	-22

[a]Based on K-band imaging of an optically selected sample. [b]Based on photometric redshift. The number of galaxies (439) is the total number of galaxies in the sample. [c]Based on K-band data of an optically selected sample and on photometric redshift.

this redshift bin. Cosmic variance affecting such small areas can affect the two samples accounting for this discrepancy. In the highest redshift bin considered, $z_m \simeq 3$, the disagreement is even larger as shown in the lower right panel of Fig. 19. At this redshift, the K_s band samples rest-frame wavelengths $\lambda \sim 0.55$ μm and the large extrapolation needed to derive the rest-frame K_s-band luminosity can be strongly dependent on the best-fitting template. In this case, as suggested by the analysis we presented in Section 5, different templates could imply different LFs. However, it should be noted that the disagreement is based on the comparison of our LF with the Schechter fit found by Kashikawa et al. and not with their data points. The few data points defining their LF in the two highest redshift bins (Fig. 5 of their paper) suggest that the Schechter parameters could not be so strongly constrained and that the disagreement could be less severe.

The agreement with the K_s-band LFs derived by other authors at redshifts comparable to $z \sim 0.6$ and to 1.2 confirms the evolution we detect in the LF of galaxies in the HDF-S, i.e. a brightening $\Delta M^* \simeq -0.4$ coupled with a decrease of the number density of bright galaxies $\Delta\phi^*/\phi^* \simeq -0.65$ from $z_m \sim 0.6$ to 1.2 for $\alpha = -1.0$. At larger redshifts, the uncertainties in the estimate of rest-frame K_s-band luminosities due to the extrapolation based on the best-fitting template could affect the LF estimates and mid-IR observations would be useful. However, even if our LF at $z_m \simeq 3$ deviates from the other LFs at this redshift, these latter LFs trace the same trend we observe, suggesting that the evolution we detect at $z < 2$ extends to $z > 3$.

6.2 The J_s-band LF

Analogous results are obtained by the comparison of our J_s-band LF estimates with those previously obtained at comparable redshifts. The comparison is shown in Fig. 21 and extends down to $z_m \sim 1.2$ because no J_s-band LFs have been estimated at higher redshift by other authors. The local J_s-band LF of Cole et al. (2001; $M^*_J = -23.13$ and $\phi^* = 0.4 \times 10^{-3}$ Mpc^{-3}) and the local LF of Balogh et al. (2001; $M^*_J = -23.02$) are consistent with our LF at $z_m \sim 0.6$. Thus, as in the case of the K_s band, we do not find evidence of a strong evolution of the LF at $z < 0.6$. However, in agreement with the K_s-band LF, we point out a brightening of $M^*_{J_s}$ of about 0.2–0.3 mag from $z = 0$ to $z_m \sim 0.6$.

The J_s-band LFs obtained at $z \sim 0.5$ by the various authors show a much larger scatter than those obtained in the K_s band at comparable redshifts. As for the K_s band, our estimate agrees with the LFs of Pozzetti et al. and of Feulner et al. (2003; both based on spectroscopic redshift), while it deviates significantly from the LFs of Bolzonella et al. (2002) and of Dahlen et al. (2005). In particular, both these LFs are characterized by significantly fainter M^* (0.4 mag with respect to our LF and 0.5–0.6 mag with respect to the LF of Feulner et al. and Pozzetti et al.). Also at redshift $z_m \sim 1.2$

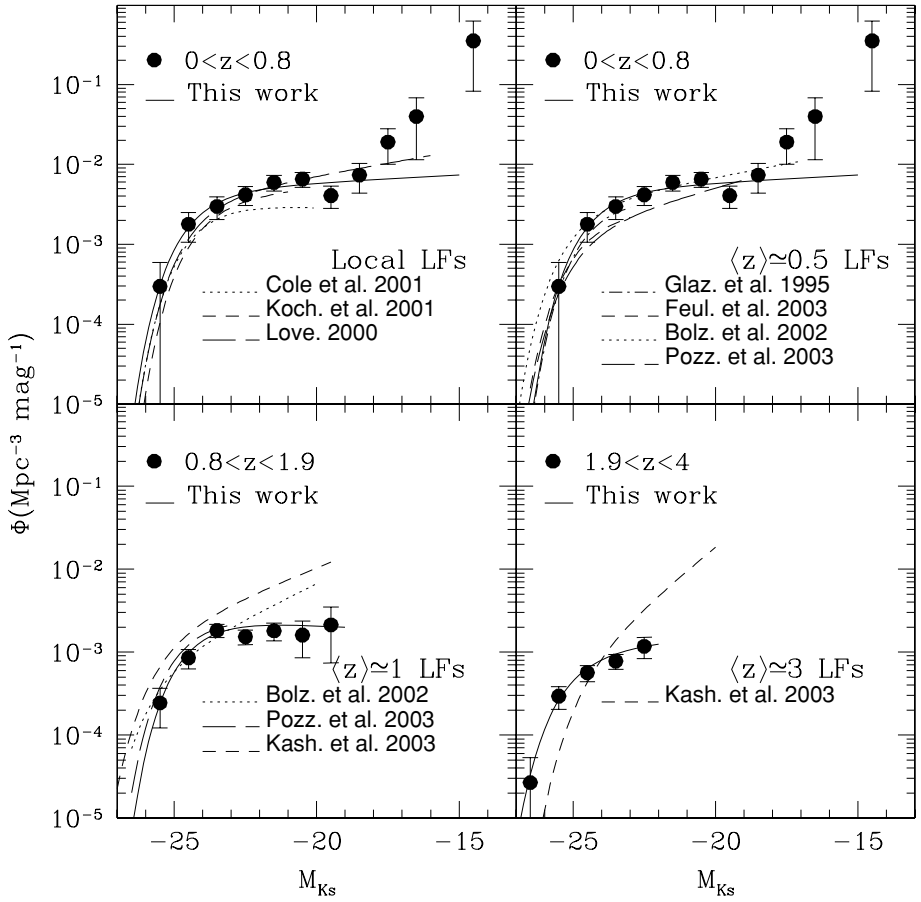

Figure 19. The rest-frame K_s-band luminosity function derived with the $1/V_{max}$ (points) and LF Schechter fitting (solid curve) are compared with the LFs obtained by various authors (Koch. = Kochaneck; Love. = Loveday; Glaz. = Glazebrook; Feul. = Feulner; Bolz. = Bolzonella; Pozz. = Pozzetti; Kash. = Kashikawa). In the upper left panel, the LF we derived in the redshift bin $z_m \simeq 0.6$ is compared with the local K-band LFs. In the other panels, our estimates are compared with those obtained by other authors at comparable redshifts: $z \simeq 0.5$ (upper right), $z \simeq 1$ (lower left) and $z \simeq 3$ (lower right).

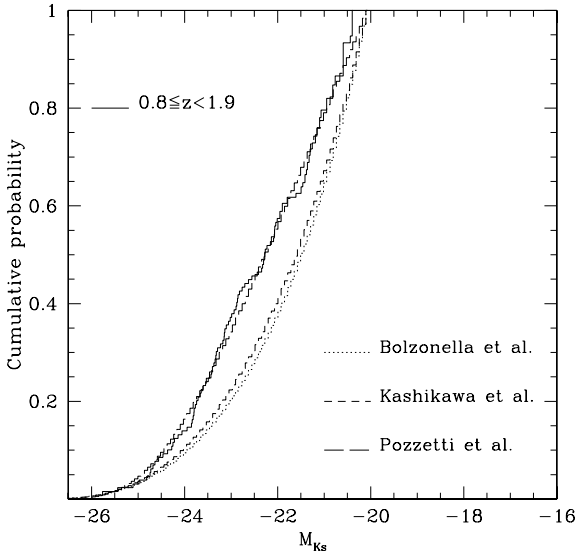

Figure 20. Comparison among the cumulative LFs derived at $z \simeq 1.2$ normalized over the same range of absolute magnitudes. The solid histogram is the CLF we derived with the $1/V_{max}$. The probability that the cumulative distributions derived by the LF of Bolzonella et al. (2002) (dotted line) and of Kashikawa et al. (2003) (dashed line) are drawn from the population our LF belongs to is less than 1 per cent.

our LF agrees very well the Pozzetti et al. LFS, while it deviates significantly from the LFs of Bolzonella et al. and Dahlen et al. These latter LFs find also an evolution of M^* in the opposite sense with respect to what we and other authors found, i.e. a dimming from $z \sim 0.4$ to 0.9. They use equation (2) to derive the rest-frame absolute magnitudes. They suggest that a negative evolution should be expected in J_s and at longer wavelengths by extrapolating the results obtained by Ilbert et al. (2005), who find that the evolution of M^* is systematically weaker from U to I bands. Thus, a turnover in the evolution of M^* could be expected at $\sim J$ and a negative evolution should take place at longer wavelengths. They suggest that the positive evolution that is instead observed by many authors is explained by the method used to derive the rest-frame luminosities we discussed in Section 4: the observed band (K_s or J_s) samples shorter rest-frame wavelengths (where the evolution is stronger) at higher redshift and the use of equation (1) to derive the rest-frame luminosities could mimic a brightening in M^*. However, we have shown in Sections 4 and 5 that this is not true at least down to $z \sim 2$ and we can consequently exclude with certainty that the evolution found by us and by other authors is due to a wrong derivation of the rest-frame luminosities.

Thus, from the comparison with the other LFs in the J_s band, we confirm an evolution in the LF of galaxies from $z_m \sim 0.6$ to 1.2, i.e. a brightening $\Delta M^* \simeq -0.4$ coupled with a decrease of the number density of bright galaxies. This evolutionary trend extends to $z \sim 3$

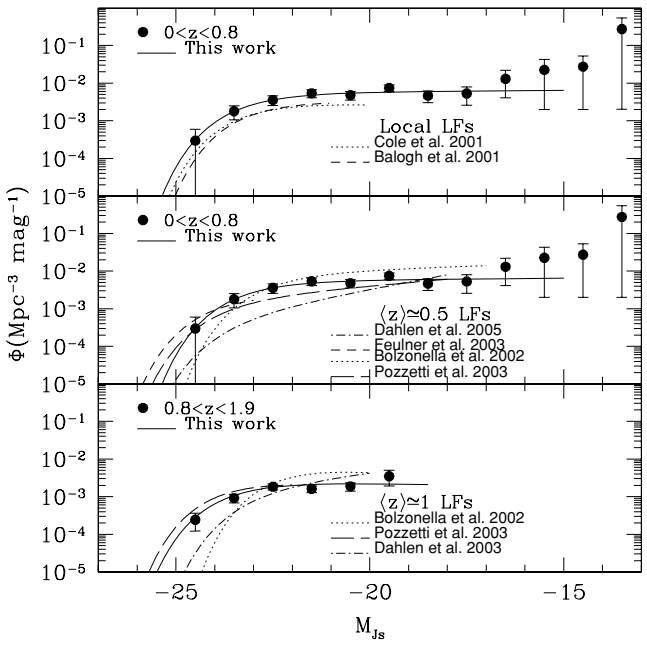

Figure 21. The rest-frame J_s-band LF derived with the $1/V_{max}$ (points) and LF Schechter fitting (solid curve) are compared with the LFs obtained by various authors. In the upper panel, the LF in the redshift bin $z_m \simeq 0.6$ is compared with the local J-band LFs. In the other panels, our estimates are compared with those obtained by other authors at comparable redshifts: $z \simeq 0.5$ (middle panel) and $z \simeq 1$ (lower panel).

even if, as for the K_s-band LF, mid-IR observations would be needed to confirm the trend.

7 SUMMARY AND CONCLUSIONS

We have probed the evolution of the rest-frame J_s- and K_s-band LFs of field galaxies with a complete sample of about 300 galaxies selected in the HDF-S at $K_s \leqslant 23$ (Vega). Photometric redshifts have been obtained from template SED fitting to U_{300}, B_{450}, V_{606}, I_{814}, J_s, H and K_s photometry after having calibrated and optimized the procedure and the set of templates with a control sample of 232 spectroscopic redshifts, 151 from the HDF-N and 81 from the HDF-S. The accuracy in the redshift estimate we obtained is 0.06 (rms).

We investigate the reliability of the rest-frame near-IR absolute magnitudes obtained using the conventional method based on the extrapolation of the observed photometry on the best-fitting template and using the photometry approaching the rest-frame near-IR. We find that the rest-frame J_s-band absolute magnitudes obtained through the photometry in the redder bands (H and K_s according to the redshift of the galaxy) are consistent with those obtained from the J_s-band photometry at least down to $z \sim 2$. This shows that the LF is not dependent either on the extrapolation made on the best-fitting template or on the library of models used.

We derived the J_s- and the K_s-band LF in the three redshift bins (0, 0.8), (0.8, 1.9) and (1.9, 4) centred at the median redshift $z_m \sim 0.6$, 1.2 and 3. Each bin contains 101, 100 and 84 galaxies of which there are 52 (50 per cent), 12 (12 per cent) and 10 (12 per cent) with spectroscopic redshift, respectively. The analysis of the observed LF at different redshifts and the comparison with those previously found by other authors at comparable redshifts and at $z = 0$ provided the following results.

(i) We find hints of a rise of the faint end ($M_{J_s} > -17$ and $M_{K_s} > -18$) of the near-IR LF at $z_m \sim 0.6$. The rise is defined by nine galaxies at $z < 0.3$ with irregular morphology as found for the local LF at an optical wavelength (e.g. Marzke et al. 1994; Zucca et al. 1997; Marzke et al. 1998; Folkes et al. 1999). They account for a comoving number density $\bar{n} = 0.4 \pm 0.23\,\mathrm{Mpc}^{-3}$ at $\langle z \rangle \simeq 0.2$, almost 1 order of magnitude higher than that of brighter galaxies. However, given the low statistics, such rise of the faint end needs a larger sample to be established.

(ii) We find no evidence of a steepening with redshift of the near-IR LFs of galaxies in the HDF-S. The value of α we find is consistent with the local value. Given the size of our sample, we estimate that, if α changes with redshift, its evolution is constrained within ± 0.3 from $z \sim 0$ to 3.

(iii) We do not find evidence of strong evolution of the LF up to $z_m \simeq 0.6$, where 50 per cent of our galaxies has spectroscopic redshift. The comparison with the local estimates of the near-IR LF (Cole et al. 2001; Kochanek et al. 2001) shows that M^* has evolved not more than 0.2–0.3 mag in this redshift range, while the number density of galaxies (ϕ^*) has not evolved significantly in this redshift range, in agreement with the previous studies (e.g. Glazebrook et al. 1995; Drory et al. 2003; Feulner et al. 2003; Pozzetti et al. 2003; Caputi et al. 2004, 2005).

(iv) We clearly detect an evolution of the LF at $z_m > 0.6$ characterized by a brightening of M^* of about 0.6 and a decrease of ϕ^* by a factor 2–3 to $z_m \sim 1.2$ both in the J_s and K_s bands. By fixing $\alpha = 1.0$, this evolution is characterized by $\Delta M^* \simeq -0.6$ (at 1σ) coupled with $\Delta\phi^*/\phi^* \simeq -0.65$ (at $> 3\sigma$). The brightening persists (at 1σ) up to $z_m \sim 3$ together with the decline of ϕ^* (at $\sim 2\sigma$) even if at a lower extent.

Our results agree, at least qualitatively, with most of the analysis previously done (Drory et al. 2003; Feulner et al. 2003; Pozzetti et al. 2003; Caputi et al. 2004, 2005) while they deviate from the recent estimate of Dahlen et al. (2005). It is worth noting the very good agreement between our LF and the one recently obtained by Caputi et al. (2006) on the Great Observatories Origins Deep Surveys (GOODS). Taking into account that the near-IR light is rather tightly connected to the stellar mass, our results can give insights into the evolution of the stellar mass of the galaxies besides their luminosity. Up to $z \simeq 0.8$, clearly little luminosity evolution and no density evolution is observed. This suggests that the population of local bright galaxies was already formed at $z \sim 0.8$ and that their stellar mass growth was already completed at this redshift. This agrees with the results on the evolution of the stellar mass density obtained by many authors: Fontana et al. (2003) and Rudnick et al. (2003) in the HDF-S, Fontana et al. (2004) on the K20 sample (Cimatti et al. 2002), Yamada et al. (2005) in the Subaru Deep Survey Field, Bundy, Ellis & Conselice (2005) and Drory et al. (2005) in the GOODS and FORS Deep Field (FDF) fields and Feulner et al. (2005a) in the Munich Near-IR Cluster Survey (MUNICS) fields. Indeed, all of them find very little or even no evolution in the stellar mass function of galaxies and in the specific star formation rate (SSFR) at $z < 1$ for high-mass galaxies.

At $z > 0.8$, the evolution is stronger and the larger brightening observed is accompanied by a decrease of the number density of bright/massive galaxies. In the redshift bin (0.8, 1.9), the number density of bright galaxies is ~30–50 per cent of the local value and reaches ~20–30 per cent at $1.9 < z < 4$. This decline in the number density suggests that up to 70 per cent of the local massive/bright galaxies has grown at $1 < z < 2$–3 through star formation, merging or both. Thus, we should expect to observe massive star-forming

galaxies with disturbed/irregular morphology and merging systems in this high-redshift range, as indeed found in same cases (e.g. Daddi et al. 2004). On the other hand, the observed evolution implies also that at least 30 per cent of the local bright/massive galaxies was already in place at $1 < z < 2$ as indeed found by some authors (Fontana et al. 2004; Förster Schreiber et al. 2004; Glazebrook et al. 2004). Pozzetti et al. (2003) and Caputi et al. (2005a) show that the bright end of the LF is dominated by early-type galaxies and that their contribution to the bright end does not decline with redshift. Thus, that 30 per cent should be dominated by early-types, implying that we should observe massive evolved galaxies fully assembled at $1 < z < 2$ and even at $z > 2$. This is indeed observed by many authors (Cimatti et al. 2004; McCarthy et al. 2004; Saracco et al. 2004; Daddi et al. 2005; Labbè et al. 2005; Longhetti et al. 2005; Saracco et al. 2005). It is worth noting that this picture could be accounted for, at least qualitatively, in the hierarchical picture of galaxy formation as suggested by the recent results obtained by Nagamine et al. (2005).

From these considerations, we can gather that the growth of massive galaxies does not follow a unique way but displays different behaviours. A significant fraction (50–70 per cent) of the brighetst/most massive galaxies increases their stellar mass over a large redshift range at $z > 1$. The remaining fraction reaches their final mass in a narrower redshift range at $z > 3$ because it is already in place by this redshift. This suggests that, for the former, the stellar mass growth has been less efficient and has proceeded more slowly than for the latter. In contrast, in the latter, the stellar mass has to be grown rapidly in a short interval, surely much shorter than 1 Gyr given their redshift. This is supported by the recent results derived by mid-IR massive galaxies observed at high z (e.g. Caputi et al. 2005b) and suggests a high efficiency in the accretion of the stellar mass in massive haloes in the early Universe, possibly through a very efficient star formation. The recent results obtained on the evolution of the SSFR of galaxies seems to point towards this direction. The strong increase in the SSFR of the most massive galaxies with redshift (Feulner et al. 2005b) favours indeed an efficient SFR in the brightest galaxies at $z > 3$–4 constraining their growth in a very short interval.

ACKNOWLEDGMENTS

This work is based on observations made with the ESO-VLT telescopes at the Paranal Observatory under the programmes 164.O-0612 and 70.B-0144 and with the NASA/ESA *Hubble Space Telescope*. We thank the anonymous referee for the useful comments, which improved the presentation of the results.

REFERENCES

Balogh M. L., Christlein D., Zabludoff A. I., Zaritsky D., 2001, ApJ, 557, 117
Bell E. F., McIntosh D. H., Katz N., Weinberg M. D., 2003, ApJS, 149, 289
Bell E. F. et al., 2004, ApJ, 608, 752
Bertin E., Arnouts S., 1996, A&AS, 117, 393
Blanton M. R. et al., 2003, ApJ, 592, 819
Bolzonella M., Miralles J.-M., Pellò R., 2000, A&A, 363, 476
Bolzonella M., Pellò R., Maccagni D., 2002, A&A, 395, 443
Bruzual A. G., Charlot S., 2003, MNRAS, 344, 1000 (BC03)
Bundy K., Ellis R. S., Conselice C. J., 2005, ApJ, 625, 621
Calzetti D., Armus L., Bohlin R. C., Kinney A. L., Koornneef J., Storchi-Bergmann T., 2000, ApJ, 533, 682
Caputi K. I., Dunlop J. S., McLure R. J., Roche N. D., 2004, MNRAS, 353, 30
Caputi K. I., Dunlop J. S., McLure R. J., Roche N. D., 2005a, MNRAS, 361, 607
Caputi K. I. et al., 2005b, ApJ, in press, astro-ph/0510070
Caputi K. I., McLure R. J., Dunlop J. S., Cirasuolo M., Schael A. M., 2006, MNRAS, 366, 609
Casertano S. et al., 2000, AJ, 120, 2747
Cimatti A. et al., 2002, A&A, 392, 395
Cimatti A. et al., 2004, Nat, 430, 184
Cohen J. G. et al., 2000, ApJ, 538, 29
Cole S. et al., 2001, MNRAS, 326, 255
Coleman G. D., Wu C.-C., Weedman D. W., 1980, ApJS, 43, 393
Cowie L. L., Songaila A., Hu E. M., Cohen J. G., 1996, AJ, 112, 839
Daddi E. et al., 2004, ApJ, 600, L127
Daddi E. et al., 2005, ApJ, 626, 680
Dahlen T., Mobasher B., Somerville R. S., Moustakas L. A., Dickinson M., Ferguson H. C., Giavalisco M., 2005, ApJ, 631, 126
Dawson S., Stern D., Bunker A. J., Spinrad H., Dey A., 2001, AJ, 122, 598
Drory N., Bender R., Feulner G., Hopp U., Maraston C., Snigula J., Hill G. J., 2003, ApJ, 595, 698
Drory N., Salvato M., Gabash A., Bender R., Hopp U., Feulner G., Pannella M., 2005, ApJ, 619, L131
Fernández-Soto A., Lanzetta K. M., Chen H.-W., Levine B., Yahata N., 2002, MNRAS, 330, 889
Feulner G., Bender R., Drory N., Hopp U., Snigula J., Hill G. J., 2003, MNRAS, 342, 605
Feulner G., Goranova Y., Drory N., Hopp U., Bender R., 2005a, MNRAS, 358, L1
Feulner G., Gabasch A., Salvato M., Drory N., Hopp U., Bender R., 2005b, ApJ, 633, L9
Fioc M., Rocca-Volmerange B., 1997, A&A, 326, 950
Folkes S. et al., 1999, MNRAS, 308, 459
Fontana A. et al., 2003, ApJ, 594, L9
Fontana A. et al., 2004, A&A, 424, 23
Förster Schreiber N. M. et al., 2004, ApJ, 616, 40
Franx M. et al., 2000, Messenger, 99, 20
Gabasch A. et al., 2004, A&A, 421, 41
Gardner J. P., Sharples R. M., Frenk C. S., Carrasco B. E., 1997, ApJ, 480, L99
Giallongo E. et al., 2005, ApJ, 622, 116
Glazebrook K., Peacock J. A., Miller L., Collins C. A., 1995, MNRAS, 275, 169
Glazebrook K. et al., 2004, Nat, 430, 181
Huang J.-S., Glazebrook K., Cowie L. L., Tinney C., 2003, ApJ, 584, 203
Ilbert O. et al., 2005, A&A, 439, 863
Kashikawa N. et al., 2003, AJ, 125, 53
Kauffmann G., Charlot S., 1998, MNRAS, 297, L23
Kochanek C. S. et al., 2001, ApJ, 560, 566
Kurucz L., 1993, http://www.stsci.edu/hst/observatory/cdbs/k93models.html
Labbè I. et al., 2003a, AJ, 125, 1107
Labbè I. et al., 2003b, ApJ, 591, L95
Labbè I. et al., 2005, ApJ, 624, L81
Lilly S. J., Tresse L., Hammer F., Crampton D., Le Fevre O., 1995a, ApJ, 455, 108
Lilly S. J., Le Fevre O., Crampton D., Hammer F., Tresse L., 1995b, ApJ, 455, 50
Lin H., Yee H. K. C., Carlberg R. G., Ellingson E., 1997, ApJ, 475, 494
Liu C. T., Green R. F., Hall P. B., Osmer P. S., 1998, AJ, 116, 1082
Longhetti M. et al., 2005, MNRAS, 361, 897
Loveday J., 2000, MNRAS, 312, 557
McCarthy P. J. et al., 2004, ApJ, 614, L9
Madgwick D. S. et al., 2002, MNRAS, 333, 133
Mannucci F., Basile F., Poggianti B. M., Cimatti A., Daddi E., Pozzetti L., Vanzi L., 2001, MNRAS, 326, 745
Maraston C., 2005, MNRAS, 362, 799 (M05)
Marzke R. O., Geller M. J., Huchra J., Corwin H. G., Jr, 1994, AJ, 108, 437
Marzke R. O., da Costa L. N., Pellegrini P. S., Willmer C. N. A., Geller M. J., 1998, ApJ, 503, 617

Mobasher B., Sharples R. M., Ellis R. S., 1993, MNRAS, 263, 560
Nagamine K., Cen R., Hernquist L., Ostriker J. P., Springer F., 2005, ApJ, 627, 608
Norberg P. et al., 2002, MNRAS, 336, 907
Poli F. et al., 2003, ApJ, 593, L1
Pozzetti L. et al., 2003, A&A, 402, 837
Prévot M. L., Lequeux J., Prévot L., Maurice E., Rocca-Volmerange B., 1984, A&A, 132, 389
Rigopoulou D., Vacca W. D., Berta S., Franceschini A., Aussel H., 2005, A&A, 440, 61
Rix H., Riecke M. J., 1993, ApJ, 418, 123
Rudnick G. et al., 2003, ApJ, 599, 847
Saracco P., Giallongo E., Cristiani S., D'Odorico S., Fontana A., Iovino A., Poli F., Vanzella E., 2001, A&A, 375, 1
Saracco P. et al., 2004, A&A, 420, 125
Saracco P. et al., 2005, MNRAS, 357, L40
Sawicki M., Mallén-Ornelas G., 2003, AJ, 126, 1208
Schechter P.,, 1976, ApJ, 203, 297
Schmidt M., 1968, ApJ, 151, 193
Szokoly G. P., Subbarao M. U., Connolly A. J., Mobasher B., 1998, ApJ, 492, 452
Takeuchi T. T., Yoshikawa K., Ishii T. T., 2000, ApJS, 129, 1
Trujillo I. et al., 2004, ApJ, 604, 521
Vanzella E. et al., 2001, AJ, 122, 2190
Vanzella E. et al., 2002, A&A, 396, 847
Wolf C., Meisenheimer K., Rix H. W., Borch A., Dye S., Kleinheinrich M., 2003, A&A, 401, 73
Yamada T. et al., 2005, ApJ, 634, 861
Zucca E. et al., 1997, A&A, 326, 477

This paper has been typeset from a TEX/LATEX file prepared by the author.